Review

Molecular Simulations and Drug Discovery of Adenosine Receptors

Jinan Wang [†] , Apurba Bhattarai [†] , Hung N. Do, Sana Akhter and Yinglong Miao *

Center for Computational Biology and Department of Molecular Biosciences, University of Kansas, Lawrence, KS 66047, USA; jawang@ku.edu (J.W.); apurba.bhattarai@ku.edu (A.B.); hungd238@ku.edu (H.N.D.); sana_email@ku.edu (S.A.)
* Correspondence: miao@ku.edu
† These authors contributed equally to this work.

Abstract: G protein-coupled receptors (GPCRs) represent the largest family of human membrane proteins. Four subtypes of adenosine receptors (ARs), the A_1AR, $A_{2A}AR$, $A_{2B}AR$ and A_3AR, each with a unique pharmacological profile and distribution within the tissues in the human body, mediate many physiological functions and serve as critical drug targets for treating numerous human diseases including cancer, neuropathic pain, cardiac ischemia, stroke and diabetes. The A_1AR and A_3AR preferentially couple to the $G_{i/o}$ proteins, while the $A_{2A}AR$ and $A_{2B}AR$ prefer coupling to the G_s proteins. Adenosine receptors were the first subclass of GPCRs that had experimental structures determined in complex with distinct G proteins. Here, we will review recent studies in molecular simulations and computer-aided drug discovery of the adenosine receptors and also highlight their future research opportunities.

1. Introduction

Adenosine (ADO) is an endogenous nucleoside, which regulates multiple biological functions by activating adenosine receptors (ARs) [1–3]. ARs belong to the class A G protein-coupled receptors (GPCRs), representing primary targets of approximately 1/3 of marketed drugs [4]. Four subtypes of ARs are expressed in human bodies, including A_1AR, $A_{2A}AR$, $A_{2B}AR$ and A_3AR. The A_1AR and $A_{2A}AR$ are high-affinity receptors for ADO, whereas $A_{2B}AR$ and A_3AR are low-affinity receptors (Table 1) [5,6].

During function, the A_1AR preferentially couples to the $G_{i/o}$ proteins to inhibit the production of cAMP by regulating the activity of adenylyl cyclase (AC) [3,7]. It could regulate many cellular responses, such as inhibition of Ca^{2+} conductance and stimulation of phospholipase C, K^+ conductance, phosphoinositide 3 kinase (PI3K) and mitogen-activated protein kinase (MAPK) [8,9] (Table 1). The A_1AR is thus considered as a potential drug target for treating myocardial ischemia [10], cardiovascular disorders [11,12], obesity [13] and cancers [14,15]. Particularly, one agonist and four antagonists of A_1AR were approved in the market (Table 1).

The $A_{2A}AR$ prefers to couple to the G_s protein to activate AC, resulting in the activation of cAMP-dependent protein kinase A (PKA), protein kinase C (PKC), MAPK and ion channels (Table 1) [16]. The $A_{2A}AR$ is widely considered as a potential drug target for treating cardiovascular disorders [11,12], obesity [13], Parkinson's disease (PD) [17,18] and cancers [14,15]. Particularly, a selective $A_{2A}AR$ antagonist Istradefylline was approved for the treatment of PD [19].

The $A_{2B}AR$ binds with the G_s and G_q proteins to induce the PKA signaling to increase the level of cAMP and stimulate phospholipase C and MAPK [20]. The $A_{2B}AR$ is recog-

nized as a drug target for treating inflammation [21,22], chronic obstructive pulmonary disease [23] and diabetes [24].

Table 1. Signaling and approved drugs of adenosine receptors.

Name	A_1AR		$A_{2A}AR$		$A_{2B}AR$	A_3AR
G protein coupling	G_i, G_o		G_s		G_s, Gq/11	G_o, $G_{q/11}$
Downstream signaling	$\downarrow$AC		$\uparrow$AC		$\uparrow$AC	$\downarrow$AC
	$\uparrow$Phospholipase C		$\uparrow$MAP Kinase		$\uparrow$Phospholipase C	$\uparrow$Phospholipase C
	$\uparrow$K$^+$ channel, $\downarrow$Ca^{2+} channel		$\uparrow$PKA		$\uparrow$PKA	$\uparrow$Ca^{2+} channel
	$\uparrow$PI3K		$\uparrow$PKC		$\uparrow$MAP Kinase	$\uparrow$PI3K
	$\uparrow$MAP Kinase					$\uparrow$PKC
						$\uparrow$MAP kinase
Adenosine binding affinity	5.10 nM		30.9 nM		1000 nM	100 nM
Approved drugs	Drug	Therapeutic use	Drug	Therapeutic use		
	Adenosine (agonist)	Paroxysmal supraventricular tachycardia	Adenosine (agonist)	Myocardial perfusion imaging		
	Regadenoson (antagonist)	Asthma	Istradefylline (antagonist)	Parkinson's disease		
	Theophylline (antagonist)	Asthma				
	Doxofylline (antagonist)	Asthma				
	Bamifylline (antagonist)	Asthma				

The A_3AR couples to the G_i protein to inhibit AC and decrease cAMP accumulation and PKA activity. Additionally, the A_3AR could bind with the G_q protein to stimulate phospholipase C, resulting in increased Ca^{2+} levels and modulation of PKC activity [25]. In addition, they may activate the phospholipase C pathway through the $G_{\beta\gamma}$ subunit [26]. Increasing attention is paid to the A_3AR for the drug development against inflammation [27], glaucoma [28], rheumatoid arthritis [29] and stroke [30].

Advances of techniques in X-ray crystallography, cryo-electron microscopy (cryo-EM) and Nuclear Magnetic Resonance (NMR) have generated a number of structures for GPCRs including the ARs. They have stimulated numerous structure-based and computer-aided drug design (CADD) developments for ARs [31]. To date (January 2022), Protein Data Bank (PDB) [32] has recorded approximately 64 structures of ARs under different functional states (Table 2). However, there has been no experimental structure for $A_{2B}AR$ and A_3AR yet. Additionally, only static snapshots of ARs could be captured in the PDB structures. It is still challenging for experimental techniques to probe flexibility of the ARs, which plays a critical role in regulating their biological functions and designing potent and selective drug molecules. Molecular dynamics (MD) simulations [33] have proven useful to model protein dynamics and ligand binding/dissociation processes, which has greatly facilitated the rational drug design targeting ARs. Here, we present a review of simulation studies that have revealed important insights into the dynamic and functional mechanisms of ARs, as well as drug discovery efforts targeting the ARs.

Table 2. The available experimental structures of the A_1AR and $A_{2A}AR$ deposited in the Protein Data Bank (PDB) along with their PDB accession codes, conformational states (inactive, partially active or fully active), the functional effect (agonist or antagonist) of the co-crystallized ligand.

PDB Code	Resolution (Å)	Binding Affinity	Receptor's States	Ligand	Reference
			A_1AR		
5UEN	3.2	IC50: 24.9 nM [34]	Inactive	Antagonist (DU172)	Glukhova et al. [35]
5N2S	3.3	Ki: 0.7 nM [36]	Inactive	Antagonist (PSB36)	Cheng et al. [36]
6D9H	3.6	Ki: 5.10 nM [37]	Active	Agonist (adenosine)	Draper-Joyce et al. [38]
7LD3	3.2	Ki: 5.10 nM [37]	Active	Agonist (adenosine)	Draper-Joyce et al. [39]
7LD4	3.3	-	Active	Agonist and PAM (adenosine and MIPS521)	Draper-Joyce et al. [39]
			$A_{2A}AR$		
7MR5	2.8	Ki: 0.1 nM [40]	Inactive	Antagonist (ZM241385)	Martynowycz et al. [41]
7ARO	3.1	-	Inactive	Partial agonist (LUF5833)	Amelia et al. [42]
6LPL	2.0	Ki: 0.1 nM [40]	Inactive	Antagonist (ZM241385)	Ihara et al. [43]
6LPK	1.8	Ki: 0.1 nM [40]	Inactive	Antagonist (ZM241385)	Ihara et al. [43]
6LPJ	1.8	Ki: 0.1 nM [40]	Inactive	Antagonist (ZM241385)	Ihara et al. [43]
6WQA	2.0	Ki: 0.1 nM [40]	Inactive	Antagonist (ZM241385)	Lee et al. [44]
6ZDV	2.1	pKD: 5.90 [45]	Inactive	Antagonist (PubChem CID 984073)	Jespers et al. [45]
6ZDR	1.9	pKD: 8.60 [45]	Inactive	Antagonist (PubChem CID 740769)	Jespers et al. [45]
6S0L	2.7	Ki: 0.1 nM [40]	Inactive	Antagonist (ZM241385)	Nass et al. [46]
6S0Q	2.7	Ki: 0.1 nM [40]	Inactive	Antagonist (ZM241385)	Nass et al. [46]
6PS7	1.9	Ki: 0.1 nM [40]	Inactive	Antagonist (ZM241385)	Ishchenkoa et al. [47]
6JZH	2.3	Ki: 0.1 nM [40]	Inactive	Antagonist (ZM241385)	Shimazu et al. [48]
6GT3	2.0	Ki: 1.7 nM [49]	Inactive	Antagonist (AZD4635)	Borodovsky et al. [49]
6MH8	4.2	Ki: 0.1 nM [40]	Inactive	Antagonist (ZM241385)	Martin-Garcia et al. [50]
6GDG	4.1	Ki: 20 nM [51]	Active	Agonist (NECA)	García-Nafría et al. [52]
5WF5	2.6	Ki: 17.3 nM [53]	Active	Agonist (UK-432097)	White et al. [53]
5WF6	2.9	Ki: 17.3 nM [53]	Active	Agonist (UK-432097)	White et al. [53]
5OLH	2.6	pkD: 9.0 [54]	Inactive	Antagonist (Vipadenant)	Rucktooa et al. [54]
5OM1	2.1	pkD: 9.6 [54]	Inactive	Antagonist (PubChem CID 135566609)	Rucktooa et al. [54]
5OLG	1.9	Ki: 0.1 nM [40]	Inactive	Antagonist (ZM241385)	Rucktooa et al. [54]
5OLO	3.1	Ki: 0.3 nM [55]	Inactive	Antagonist (Tozadenant)	Rucktooa et al. [54]
5OM4	2.0	Ki: 1.41 nM [56]	Inactive	Antagonist (PubChem CID 135566609)	Rucktooa et al. [54]
5OLV	2.0	Ki: 5.9 nM [57]	Inactive	Antagonist (CHEMBL 1671936)	Rucktooa et al. [54]
5OLZ	1.9	Ki: 1.51 nM [56]	Inactive	Antagonist (PubChem CID 135566609)	Rucktooa et al. [54]
6AQF	2.5	Ki: 0.10 nM [40]	Inactive	Antagonist (ZM241385)	Eddy et al. [58]
5VRA	2.4	Ki: 0.10 nM [40]	Inactive	Antagonist (ZM241385)	Broecker et al. [59]

Table 2. *Cont.*

PDB Code	Resolution (Å)	Binding Affinity	Receptor's States	Ligand	Reference
			$A_{2A}AR$		
5NM2	2.0	Ki: 0.1 nM [40]	Inactive	Antagonist (ZM241385)	Weinert et al. [60]
5NM4	1.7	Ki: 0.10 nM [40]	Inactive	Antagonist (ZM241385)	Weinert et al. [60]
5NLX	2.1	Ki: 0.10 nM [40]	Inactive	Antagonist (ZM241385)	Weinert et al. [60]
5N2R	2.8	-	Inactive	Antagonist (PSB36)	Cheng et al. [36]
5MZP	2.1	Ki: 5011.87 nM [61]	Inactive	Caffeine	Cheng et al. [36]
5MZJ	2.0	Ki: 0.60 nM [62]	Inactive	Theophylline	Cheng et al. [36]
5JTB	2.8	Ki: 0.10 nM [40]	Inactive	Antagonist (ZM241385)	Melnikov et al. [62]
5UVI	3.2	Ki: 0.10 nM [40]	Inactive	Antagonist (ZM241385)	Martin-Garcia et al. [63]
5UIG	3.5	-	Inactive	Antagonist (PubChem CID 124081196)	Sun et al. [64]
5K2A	2.5	Ki: 0.10 nM [40]	Inactive	Antagonist (ZM241385)	Batyuk et al. [65]
5K2D	1.9	Ki: 0.10 nM [40]	Inactive	Antagonist (ZM241385)	Batyuk et al. [65]
5K2C	1.9	Ki: 0.10 nM [40]	Inactive	Antagonist (ZM241385)	Batyuk et.al. [65]
5K2B	2.5	Ki: 0.10 nM [40]	Inactive	Antagonist (ZM241385)	Batyuk et al. [65]
5G53	3.4	Ki: 1.00 nM [66]	Active	Agonist (NECA)	Carpenter et al. [67]
5IU4	1.7	Ki: 0.10 nM [40]	Inactive	Antagonist (ZM241385)	Segala et al. [68]
5IU8	2.0	Ki: 18 nM [68]	Inactive	Antagonist (Q27456347)	Segala et al. [68]
5IUB	2.1	Ki: 0.35 nM [68]	Inactive	Antagonist (Q27456347)	Segala et al. [68]
5IUA	2.2	Ki: 1.5 nM [68]	Inactive	Antagonist (6DX)	Segala et al. [68]
5IU7	1.9	Ki: 1.1 nM [68]	Inactive	Antagonist (6DX)	Segala et al. [68]
4UG2	2.6	Ki: 8.80 nM [69]	Active	Agonist (CGS-21680)	Lebon et al. [70]
4UHR	2.6	Ki: 8.80 nM [69]	Active	Agonist (CGS-21680)	Lebon et al. [70]
4EIY	1.8	Ki: 0.10 nM [40]	Inactive	Antagonist (ZM241385)	Liu et al. [71]
3UZC	3.3	Kd: 0.25 nM [56]	Inactive	Antagonist (PubChem CID 135566609)	Congreve et al. [56]
3UZA	3.3	Ki: 7.76 [56]	Inactive	Antagonist (PubChem CID 56844240)	Congreve et al. [56]
3VGA	3.1	Ki: 0.10 nM [40]	Inactive	Antagonist (ZM241385)	Hino et al. [72]
3VG9	2.7	Ki: 0.10 nM [40]	Inactive	Antagonist (ZM241385)	Hino et al. [72]
3PWH	3.3	Ki: 0.10 nM [40]	Inactive	Antagonist (ZM241385)	Dore et al. [73]
3RFM	3.6	Ki: 5011.87 nM [61]	Inactive	Antagonist (Caffeine)	Dore et al. [73]
3REY	3.3	Kd: 10 nM [73]	Inactive	Antagonist (XAC)	Dore et al. [73]
2YDO	3.0	Ki: 30.9 nM [74]	Active	Agonist (adenosine)	Lebon et al. [56]
2YDV	2.6	Ki: 13.8 nM [74]	Active	Agonist (NECA)	Lebon et al. [56]
3QAK	2.7	Ki: 4.75 nM [75]	Active	Agonist (UK-432097)	Xu et al. [75]
3EML	2.6	Ki: 0.10 nM [40]	Inactive	Antagonist (ZM241385)	Jaakola et al. [76]

2. Molecular Simulations Revealed Functional Mechanisms of Adenosine Receptors

2.1. Activation of Adenosine Receptors

The classical view of GPCR activation involves conformational states between the active and inactive states [77]. Agonist binding shifts the conformational ensemble of receptor to the activated state to enable coupling of the G protein. Recent successes in

structural biology have generated many high resolution structures of ARs under both active and inactive states (Table 2 and Figure 1). Comparison between the active and inactive structures of the A_1AR [35,38] revealed a large outward movement of transmembrane helix 6 (TM6) intracellular domain during activation of the receptor, which opened the intracellular pocket for G protein binding (Figure 1). Meanwhile, the receptor activation was accompanied by adjustments of the TM7, helix 8 (H8), extracellular loops (ECLs) and ligand binding pocket (Figure 1). A number of important structural motifs, named "microswitches", play a critical role in the activation of ARs, including the $R^{3.50}$-$E^{6.30}$ salt bridge, the $W^{6.48}$ "rotamer toggle switch" and the $Y^{7.53}$ "tyrosine toggle switch" [78]. The Ballesteros–Weinstein numbering [79] is used for residues in the GPCRs. Although NMR has been used to probe populations of different activation states of the $A_{2A}AR$ [58,80,81], it remains challenging to probe dynamic conformational transitions among these different states using experimental techniques. In this regard, MD simulations have been widely applied to study the activation mechanism of ARs.

The $R^{3.50}$-$E^{6.30}$ salt bridge was very stable in MD simulations of the *apo* $A_{2A}AR$ in the inactive state [82,83]. Rotameric transition of the $W^{6.48}$ was observed in MD simulations of the agonist 5′-*N*-carboxamidoadenosine (NECA)-bound $A_{2A}AR$, which allowed for water movement through the TM bundle [84]. Such movement further induced a rotational switch of the residue $Y^{7.53}$, inward movement of TM7 on the intracellular side and outward movement of TM6, leading to the opening of the intracellular pocket to facilitate G protein binding [85]. Advances in computing hardware (e.g., GPU and Anton) and software developments have enabled longer conventional MD (cMD) simulations [86]. Even so, cMD is often limited to typically hundreds of nanoseconds to tens of microseconds [87,88]. However, activation of GPCRs including ARs is still beyond the accessible time scale of cMD, which often occurs over milliseconds or even longer timescales [89].

Enhanced sampling techniques that could observe much longer timescale events within shorter simulation time have thus been applied to explore AR activation and deactivation [90,91]. Adaptive sampling combined with Markov State Models (MSMs) allowed for calculation of the activation energy landscape of the *apo* $A_{2A}AR$. The *apo* $A_{2A}AR$ sampled four predominant states, including the inactive antagonist bound-like state, the inactive *apo* intermediate state, the agonist-competent state and the active state [92]. Moreover, Li et al. performed extensive Metadynamics simulations to explore the activation and deactivation mechanism of the $A_{2A}AR$ [93]. The $A_{2A}AR$ was simulated in the agonist-bound, antagonist-bound and *apo* forms. The simulations sampled distinct conformational states of the $A_{2A}AR$ that resembled the receptor active and inactive states, involving marked conformational transitions of the $W^{6.48}$ toggle switch. Three distinct regions in the orthostatic binding pocket were identified to be responsible for the ligand binding affinity, selectivity and agonism/antagonism, respectively. In addition, deactivation of the A_1AR was observed in our recent Gaussian accelerated molecular dynamics (GaMD) simulations of the active receptor after removing the G protein [39]. In summary, MD simulations, especially enhanced sampling, have provided unprecedented insights into the activation mechanism of ARs at the atomistic level.

2.2. Specific G Protein Coupling to Adenosine Receptors

The odd ARs (A_1AR and A_3AR) preferentially couple to the $G_{i/o}$ proteins, while the even subtypes ($A_{2A}AR$ and $A_{2B}AR$) preferentially couple to the G_s proteins. However, increasing studies suggest that GPCRs including the ARs could couple to multiple G proteins [94–97]. MD simulations were applied to investigate the dynamic AR-G protein interactions. The role of G protein in stabilizing the active state of $A_{2A}AR$ was investigated by Lee et al. [98]. Four different conformations of $A_{2A}AR$, including the inactive, active-intermediate and fully active in the presence and absence of the mini-G_s protein, were used as simulation starting structures. In comparison to the inactive state, lower agonist fluctuations and decreased entropy in the ECLs were observed in the active-intermediate state. In the fully active G protein-bound state, the entropy of ECLs was the highest. The volume of the receptor orthosteric pocket decreased to enable tighter contacts with the

agonist. This allowed the G protein-bound active conformation to have better allosteric communication between the G protein binding pocket and the orthosteric site.
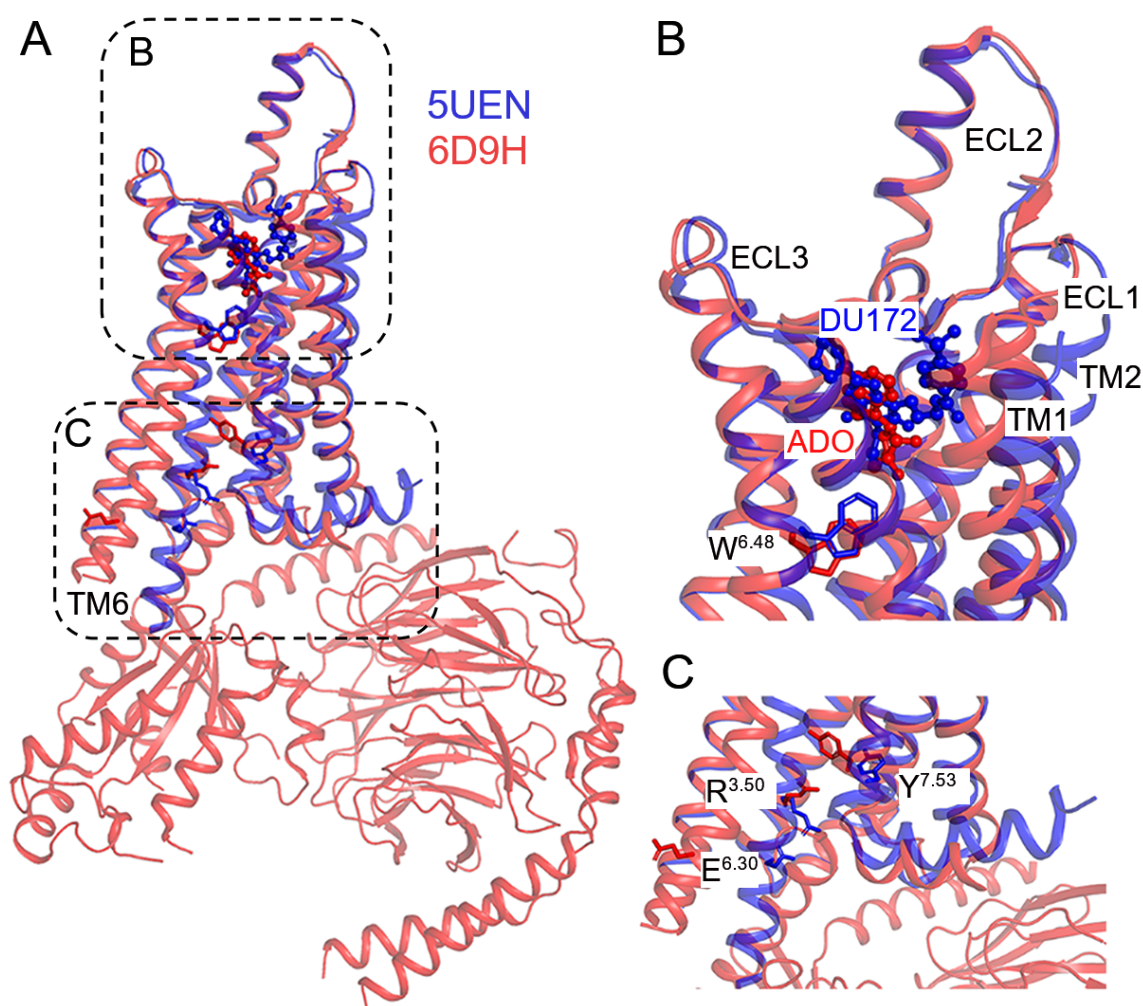

Figure 1. Comparison of experimental structures of the inactive antagonist-bound (PDB: 5UEN) and active agonist-G protein-bound (PDB: 6D9H) A_1AR. (**A**) Outward movement of transmembrane helix 6 (TM6) in the active agonist-bound receptor (red) induces opening of the intracellular pocket for binding with G protein as compared to the inactive antagonist-bound conformation of the receptor (blue). (**B**) The receptor activation is accompanied by adjustments of the ligand binding pocket, extracellular loops (ECLs) and the $W^{6.48}$ "rotamer toggle switch". Antagonist DU172 (blue) and agonist adenosine (ADO, red) occupy different regions of the orthosteric pocket in the inactive and active conformations of the A_1AR receptor, respectively. (**C**) "Microswitches" play a critical role in the activation of adenosine receptors, including the $R^{3.50}$-$E^{6.30}$ salt bridge and the $Y^{7.53}$ "tyrosine toggle switch".

In a recent study [99], we employed GaMD simulations on the cryo-EM structures of native agonist ADO-bound A_1AR-G_i and NECA-bound $A_{2A}AR$-G_s protein complexes [38,52], as well as "decoy" complexes generated by switching the G proteins (A_1AR-G_s and $A_{2A}AR$-G_i). GaMD simulations suggested that slight differences of agonist NECA binding in the $A_{2A}AR$ were observed upon changing the G_s protein to the G_i (Figure 2C), while significantly increased fluctuations in the A_1AR and ADO were identified upon changing the G_i protein to the G_s (Figure 2D). The agonist ADO sampled two different binding poses ("L1" and "L2") when the A_1AR coupled with the G_s protein. In the "L2" binding pose, ADO formed interactions with residues $Y^{1.35}$ and $Y^{7.36}$ in the sub-pocket 2 of the A_1AR as described earlier [35]. Only one stable low-energy conformation was observed for each of the A_1AR-G_i and $A_{2A}AR$-G_s complexes as

in the cryo-EM structures (Figure 2A,B), being similar for the $A_{2A}AR$-G_i complex (Figure 2C). While multiple states of the ADO agonist and G_s protein were sampled in the A_1AR-G_s system (Figure 2D). Simulation results thus indicated that the A_1AR preferred to couple with the G_i protein to the G_s (Figure 2E), while the $A_{2A}AR$ could couple with both the G_s and G_i proteins (Figure 2F), being highly consistent with experimental findings of the ARs [94–96]. Further detailed analysis of the simulation trajectories suggested that remarkably complementary residue interactions at the protein interface led to the specific AR-G protein coupling, which involved mainly the receptor TM6 helix, the G_α α5 helix and α4-β6 loop. In summary, the GaMD simulations have provided important insights into the dynamic mechanism of specific GPCR-G protein interactions.

2.3. Biased Agonism of Adenosine Receptors

Biased agonism is a phenomenon in which binding of different agonists to a target GPCR promotes distinct receptor conformations that bias cellular signaling toward and away from a subset of pathways, e.g., activation of different G protein or arrestin [100–103]. Biased agonism was first introduced by Jarpe et al. [103] and has been targeted for developing selective therapeutics of GPCRs [102,104]. The first A_1AR biased agonist LUF5589 was identified by assessing A_1AR bias with 800 A_1AR agonists and antagonists in 2013 [105]. The AR biased agonism has been explored by MD simulations. By combining MD simulations, $G\alpha i/o$ subunit- and β-arrestin-specific cellular signaling assays, Wall et al. [106] identified that the A_1AR-selective agonist, BnOCPA, was a biased agonist in exclusively activating the G_{ob} protein. MD simulations were applied on the A_1AR bound by the biased agonist BnOCPA, neutral agonists ADO and HOCPA and an antagonist PSB36. The simulations suggested that BnOCPA engaged with the same receptor interactions as neutral agonists ADO and HOCPA. However, a distinct partial transition of the $N^{7.49}PxxY^{7.53}$ backbone from the active to inactive state was observed in one of the BnOCPA-bound A_1AR simulations. The α5 helix (GαCT) of the G protein (G_{i2}, G_{oa}, G_{ob}) was dynamically docked to the HOCPA- and BnOCPA-bound active A_1AR structures to study the agonist-driven interaction between the A_1AR and the G protein. MD simulations suggested that the GαCT of G_{ob} docked to the A_1AR via a metastable state (MS1) relative to the canonical state (CS1). The CS1 corresponded to the canonical arrangement as captured in the cryo-EM structure of the A_1AR-Gi (PDB: 6D9H), whereas the MS1 was similar to the non-canonical state in the neurotensin receptor, being suggested as an intermediate on the way to the canonical state [107]. In contrast, docking of the GαCT of G_{oa} and G_{i2} to the A_1AR formed MS2 and MS3 states. The MS2 was similar to the β_2-adrenergic receptor–$G_{\alpha s}$CT complex [108], which was proposed to be an intermediate on the activation pathway and play an important role in G protein specificity. Additional MD simulations were performed on the BnOCPA- and HOCPA-bound A_1AR in complex with the entire G_{oa} and G_{ob} proteins, respectively. The main differences between the G_{oa} and G_{ob} proteins comprised the formation of transient hydrogen bonds between the α3-β5 and α4-β6 loops of G_{oa} and H8 of the A_1AR. Overall, G_{oa} interacted more with residues at the TM3 and ICL2 of receptor, while TM5, TM6 and ICL1 were more engaged by G_{ob}. Particularly, residues $R^{7.56}$ and $I^{8.47}$ showed a different propensity to interact with G_{oa} or G_{ob} proteins. Therefore, a particular A_1AR conformation stabilized by BnOCPA may favor different intermediate states during the binding process of G_{oa} and G_{ob} proteins.

In previous studies, bitopic ligands that comprise of orthosteric and allosteric ligand binding moieties were shown to exhibit biased agonism in the A_1AR [100,109]. The supervised MD (SuMD) simulations were performed to capture the binding of bitopic agonist VCP746 (biased agonist) and its allosteric part (VCP171) to the A_1AR [110]. The VCP746 sampled the most stable binding pose when the orthosteric site was occupied by the adenosine moiety, suggesting that the agonist component of the VCP746 played a particularly important role in the binding. VCP746 interacted with many receptor side chains and the ECL2 backbone atoms. The linker was captured to insert between the $E172^{ECL2}$ and $M^{5.35}$ side chains in the simulations. The allosteric moiety part VCP171 sampled many orientations on ECL2 but stabilized in a binding mode near ECL2 when the adenosine moiety reached the orthosteric binding site. Side chains $E172^{ECL2}$ and $K173^{ECL2}$ formed a sort of saddle

for the allosteric moiety, which often oriented the 3-(trifluoromethyl)phenyl group toward the hydrophobic pocket formed by residues K173^{ECL2} and I167^{ECL2}. In comparison, the positive allosteric modulator (PAM) VCP171 usually oriented its 3-(trifluoromethyl)phenyl moiety toward the top of ECL2. Taken together, these computational findings suggested a different binding mode for VCP171 as part of VCP746 and proposed an allosteric site of ECL2 as involved in the observed bias (Figure 3).
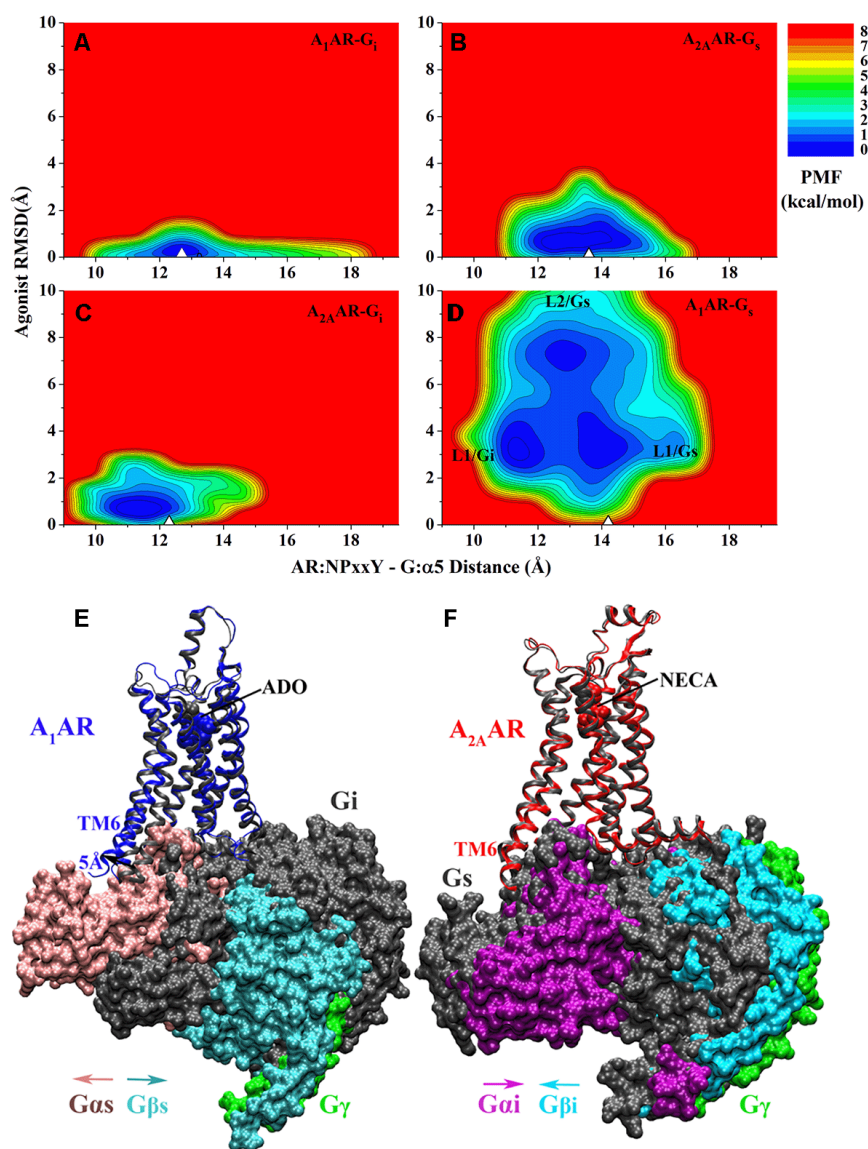

Figure 2. GaMD simulations revealed mechanism of specific G protein coupling to adenosine receptors: 2D potential of mean force (PMF) profiles of the (**A**) A$_1$AR-G$_i$, (**B**) A$_{2A}$AR-G$_s$, (**C**) A$_{2A}$AR-G$_i$ and (**D**) A$_1$AR-G$_s$ complex systems regarding the agonist RMSD relative to the cryo-EM conformation and AR:NPxxY-G:α5 distance. The white triangles indicate the cryo-EM or simulation starting structures. Summary of specific AR-G protein interactions: (**E**) the ADO-bound A$_1$AR prefers to bind the G$_i$ protein to the G$_s$. The latter could not stabilize agonist ADO binding in the A$_1$AR and tended to dissociate from the receptor. (**F**) The A$_{2A}$AR could bind both the G$_s$ and G$_i$ proteins, which adopted distinct conformations in the complexes. Adapted from reference [99] with permission from American Chemical Society. Further permissions related to the material excerpted should be directed to the American Chemical Society.
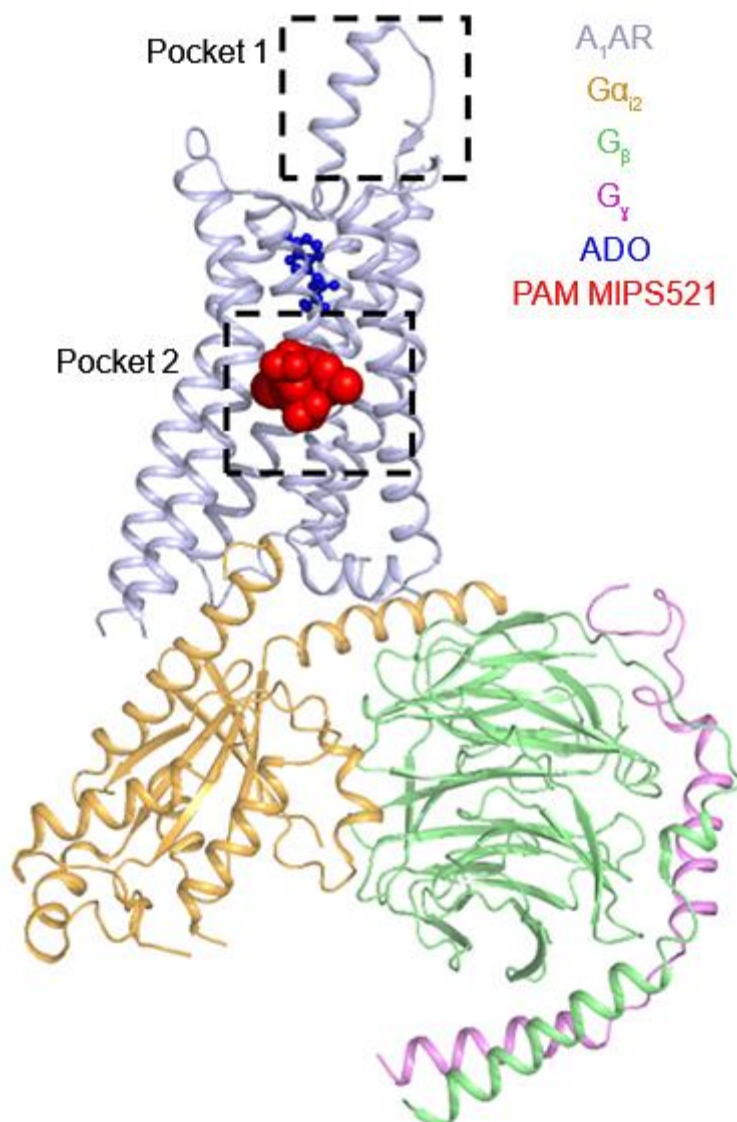
Figure 3. The "allosteric" binding sites (pocket 1 and pocket 2) in the A_1AR. The cryo-EM structure of A_1AR–Gi2 complex bound by the PAM MIPS521 (pocket 2) was shown. Another allosteric binding site (pocket 1) was suggested by mutation experiments and MD simulations.

2.4. Allosteric Modulation of Adenosine Receptors

Due to high similarity of the orthosteric site among different ARs, agonists have failed clinical trials due to off-target side effects. To overcome this problem, allosteric modulators have been developed that bind topographically distinct "allosteric" sites in the receptor (Figure 3) and regulate the effects of orthosteric ligands. PAMs potentiate the effects of orthosteric ligands, whereas negative allosteric modulators (NAMs) do the opposite. AR allosteric modulators provide subtype selectivity reducing the off-target side effects and hence represent a promising approach to selective drug design. Gao et al. [111] characterized the binding and functional antagonism of fluorescent conjugates of xanthine amine congener (XAC) and SCH442416 to the $A_{2A}AR$. Among antagonists tested, MRS7322, MRS7396, MRS7416, XAC245 and XAC630 behaved as allosteric antagonists of $A_{2A}AR$, whilst MRS7395 and XAC488 acted as competitive antagonists [111]. Allosteric antagonists MRS7396 and 5-(*N*,*N*-hexamethylene)amiloride (HMA) were more potent than MRS7416 in displacing [^{3}H]ZM241385 binding, while MRS7396, XAC630 and HMA were less potent than radioligand binding in displacing MRS7416 binding [111]. Mutation of D52N in the

sodium site of $A_{2A}AR$ changed the affinity of HMA and MRS7396, indicating preferences for different $A_{2A}AR$ conformations [111].

In one study, we performed GaMD simulations to identify binding modes of two prototypical PAMs in the A_1AR [112]. VCP171 and PD81723 were initially placed around 20 Å away from the receptor. Amber [113] and NAMD [114] software packages were used to perform enhanced sampling of PAMs binding to the receptor. GaMD predicted the binding modes of both the PAMs near ECL2 site which was consistent with the experimental mutagenesis results [115]. In the PAM-bound state of the receptor, the NECA agonist exhibited lower fluctuations in the orthosteric site. In contrast, without the PAM, the agonist was observed to be very dynamic in the orthosteric site and could even dissociate in some of the simulations.

Very recently, using the first cryo-EM structure of A_1AR bound to a PAM MIPS521 in presence of bound ADO agonist and G protein, we performed further GaMD simulations to characterize molecular basis of allosteric modulation [39]. GaMD simulations showed that the MIPS521 PAM molecule could stabilize the ADO in the orthosteric pocket (Figure 4). Even in the absence of G protein, the PAM molecule could show positive cooperativity stabilizing the ADO agonist. We could observe deactivation during GaMD simulation of A_1AR without the PAM and G protein, whereas the presence of MIP521 could slow deactivation of A_1AR without the G protein bound (Figure 4). This showed that the MIP521 PAM could stabilize the ADO-bound of A_1AR in a "G-protein-bound-like" conformation.
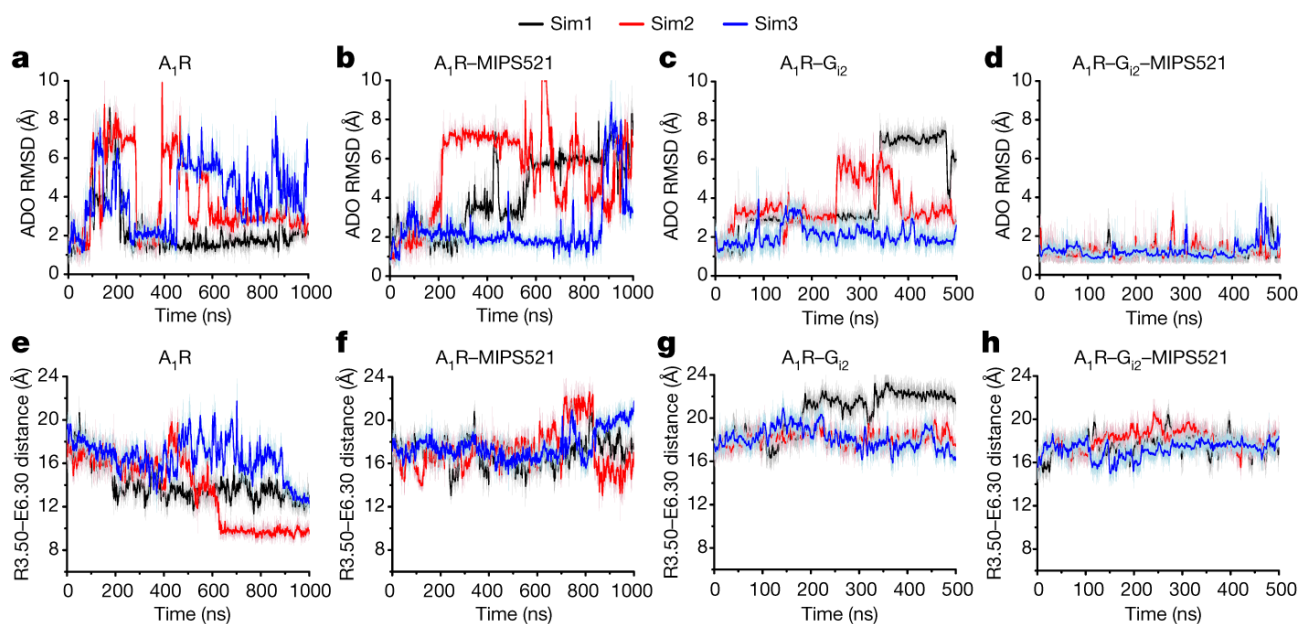

Figure 4. MIPS521 PAM molecule stabilized the ADO agonist binding and the A_1AR-G_{i2} protein complex, as well as slowing deactivation of A_1AR upon removal of the G_{i2} protein. RMSD (Å) of ADO from GaMD simulations completed in the absence (**a**) or presence (**b**) of MIPS521, G_{i2} (**c**) or both (**d**). (**e**–**h**) Distance between the intracellular ends of TM3 and TM6 (measured as the distance in Å between charge centers of residues $R^{3.50}$ and $E^{6.30}$) in the absence (**e**) or presence (**f**) of MIPS521, G_{i2} (**g**) or both (**h**). Each condition represents three GaMD simulations, with each simulation trace displayed in a different color (black, red, blue). The lines depict the running average over 2 ns. Reprinted from reference [39] with permission from Springer Nature.

SuMD simulations were also performed to investigate the binding of LUF6000 PAM to the A_3AR [116]. The SuMD simulations characterized the binding pathway of LUF6000 PAM to the A_3AR in presence of agonist ADO. In presence of the agonist, LUF6000 bound to the receptor in two different poses. First, the PAM bound to the ECL2 site changing its conformation which further induced energetically favorable agonist interactions in the

orthosteric site. Second, the PAM stably bound near the mouth of the orthosteric site stabilizing the ternary complex with agonist-bound receptor. In another study, SuMD simulations were performed to study the allosteric role of sodium ion binding to the $A_{2A}AR$ [117]. The sodium ion has been proposed as a NAM as it was observed in a distal site compared to the orthosteric site [71]. The sodium ion was able to coordinate the inactive $A_{2A}AR$ without any conformational changes in the SuMD simulations. However, the TM helices rearranged to accommodate the sodium ion in an intermediate-active state of $A_{2A}AR$. Deganutti et al. performed SuMD simulations to capture binding of the antagonist 13B, bitopic agonist VCP746 and PAMs PD81723 and VCP171 to the A_1AR [110]. The SuMD simulations showed that PAMs can bind to several receptor sites rather than a single allosteric pocket. In absence of the NECA agonist, PAM showed partial agonism behavior. Despite having structural similarities between PAMs, different binding paths were observed in the simulations, which revealed dramatic effects of subtle chemical modifications in the ligand structure.

2.5. Ligand Binding to Adenosine Receptors

Ligand binding kinetics, especially the dissociated rate, have recently been recognized to be potentially more relevant for drug design. MD simulations have been performed in order to understand ligand binding/unbinding of ARs. In a study combining MD simulations and kinetic radioligand binding experiments, Guo et al. investigated the dissociation mechanism of an antagonist ZM241385 to the $A_{2A}AR$ [118]. MD simulations that captured the dissociation of the antagonist ZM241385 from the $A_{2A}AR$ helped identify the residues in the ligand unbinding pathway. Experiments validated that mutation of these residues could influence ligand's dissociation rate dramatically even though the binding affinity was barely changed. This study demonstrates that receptor structural elements that are not important to binding affinity can prove key to ligand kinetics.

SuMD simulations were performed to study the binding interactions of ADO and its metabolite inosine ligand to the A_2AR in both the active-intermediate and its G protein-bound conformations [119]. During the SuMD simulations of ADO-bound $A_{2A}AR$, the ligand was stabilized by two hydrogen bonds formed with residues $N^{6.55}$ and $E169^{ECL2}$ in the orthosteric pocket. Conversely, inosine could form only one hydrogen bond with $N^{6.55}$. Interestingly, ligand binding in the orthosteric pocket of both systems was remarkably influenced by the presence of G protein. In another SuMD study, Sabbadin et al. explored the recognition pathway of ADO by the $A_{2A}AR$ [120]. SuMD simulations showed that ECL3 represents a possible metastable binding site for ADO. During the binding process, ECL3 helped orient the adenosine ribose ring toward orthosteric entrance. In the orthosteric binding site, ribose moiety of the ligand experienced dynamic flipping between "ribose-down" and "ribose-up" conformations. Bolcato et al. performed SuMD simulations to study binding of subtype selective antagonists LC4 and Z48 binding to A_1AR and $A_{2A}AR$, respectively [121]. The simulations showed that receptor-ligand recognitions were multistep processes involving intermediate states to guide the (un)binding events. Overall, Z48 favored $A_{2A}AR$ over A_1AR, forming classic antagonist fingerprint interactions at the orthosteric site. In case of the A_1AR, a water molecule was seen playing a key role in stabilizing LC4 at the orthosteric pocket, which was not observed in the case of $A_{2A}AR$. In another study, Deganutti et al. [122] performed SuMD simulations to investigate the binding/unbinding pathways of five different A_1AR agonists including ADO, CPA, NECA, HOCPA and BnOCPA. The SuMD simulations showed that the ligand followed the binding paths involving mainly ECL2, the top part of TM1, TM2, TM6 and TM7. The ligand dissociated following similar paths; however, ECL2 was less engaged. These pathways were further supported by alanine mutagenesis experiments.

Recently, we performed GaMD simulations to determine the binding and dissociation pathways of caffeine (CFF) antagonist to the $A_{2A}AR$ [123]. The X-ray structure of $A_{2A}AR$ in complex with CFF (PDB: 5MZP) [36] was used as initial conformation. A total of 10 CFF molecules were placed randomly at a distance >15 Å from the extracellular surface of the

A$_{2A}$AR. Spontaneous binding and dissociation of CFF in the receptor were successfully captured in the GaMD simulations. A main binding pathway of CFF to the A$_{2A}$AR was identified from the 63-ns GaMD equilibration (Figure 5A). CFF reached its binding site of the A$_{2A}$AR through interacting with ECL2, ECL3, TM7 and finally the receptor orthosteric site (Figure 5D). GaMD production simulations captured a slightly different binding pathway when the orthosteric pocket was already occupied by one CFF molecule (Figure 5B). The second CFF explored a region between ECL3 and TM7 during this binding process (Figure 5E). The dissociation pathway of CFF was mostly the reverse of the dominant binding pathway (Figure 5C,F).
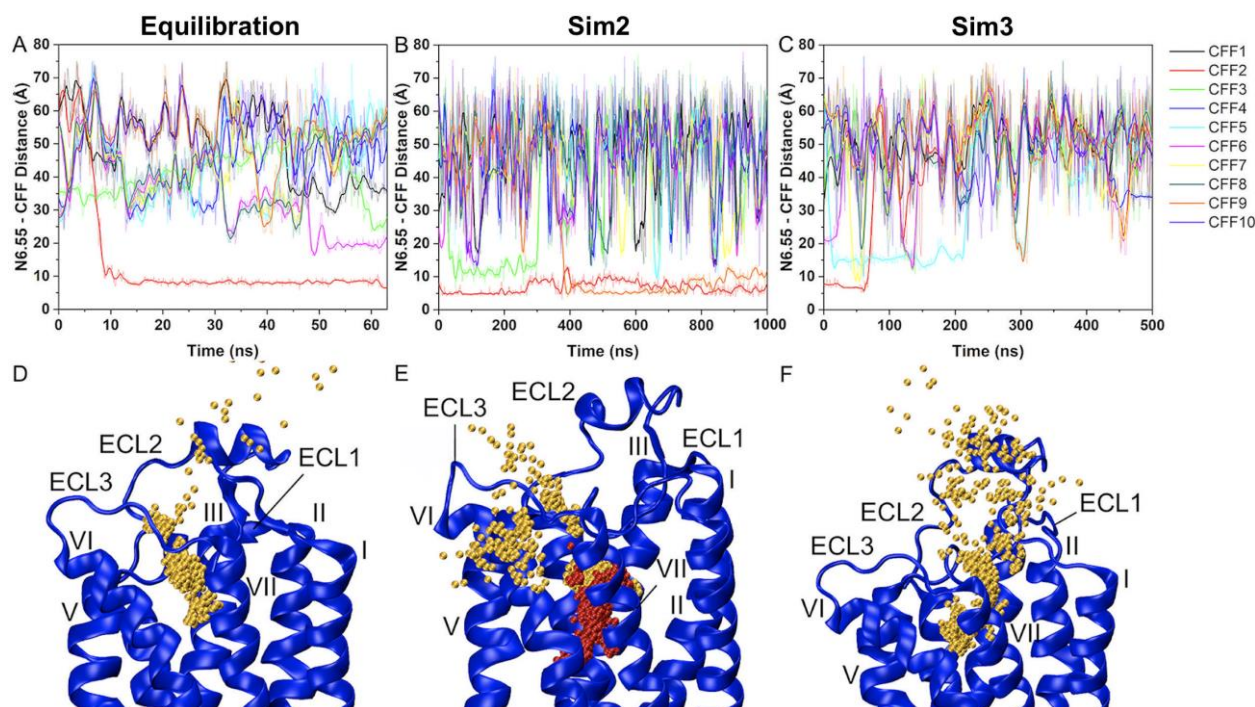
Figure 5. Binding and dissociation pathways of caffeine (CFF) from the A$_{2A}$AR were revealed from GaMD simulations. (**A–C**) Time courses of the N6.55:ND2-CFF:N1 distance calculated from GaMD equilibration, Sim2 and Sim3 GaMD production simulations. (**D–F**) Trace of CFF (orange and red) in the A$_{2A}$AR observed in the GaMD equilibration, Sim2 and Sim3 GaMD production simulations. The seven transmembrane helices are labeled I to VII, and extracellular loops 1–3 are labeled ECL1–ECL3. Reprinted from reference [123] with permission from Frontiers.

2.6. Lipid Interactions with Adenosine Receptors

Lipid bilayers have been shown to modulate GPCR functions, including conformation stability, ligand binding and oligomerization [124–126]. Modulatory effects mediated via changes in the physical properties of membrane, such as thickness, curvature and surface tension, have been extensively studied using experimental and computational methods [126,127]. Here, we discuss MD studies focusing on AR-lipid interactions.

In one study, GaMD simulations were applied to study the relationship between the lipid environment and A$_1$AR activation state [128]. The cryo-EM structure of the active ADO-bound A$_1$AR coupled with the G$_i$ protein (A$_1$AR-Gi) [38] and the X-ray structure [35,36] of the inactive antagonist PSB36-bound A$_1$AR (PSB36-A$_1$AR) were used to perform GaMD simulations. The A$_1$AR was embedded in a 1-palmitoyl-2-oleoyl-glycero-3-phosphocholine (POPC) lipid bilayer. GaMD simulations suggested that the membrane lipids play a critical role in stabilizing different states of the A$_1$AR. Different structural flexibility profiles were identified in GaMD simulations of the inactive and active A$_1$AR. Compared with the inactive A$_1$AR, higher fluctuations were found at the ECL2 region, intracellular ends of TM5 and TM6 in the active A$_1$AR. The receptor TM domain and the

ligands were rather rigid. However, the G protein coupled to the active A_1AR exhibited high flexibility, especially in the, $\alpha4$-$\beta5$ loop and $\alpha4$-$\beta6$ loop and $\alpha5$ helix of the $G\alpha$ subunit and terminal ends of the $G_{\beta\gamma}$ subunits.

The -S_{CD} order parameter values obtained from GaMD simulations agreed well with experimental data. In NMR experiments, the -S_{CD} for the fifth carbon C-H bond of POPC was at ~0.18–0.20 [129]. The -S_{CD} value of POPC's fifth carbon atom was ~0.17 $\pm$ 0.02 in the lower leaflet in the active A_1AR system. It increased to ~0.20 $\pm$ 0.02 in the inactive A_1AR system (Figure 6). The -S_{CD} value of the ninth carbon C-H bond in POPC calculated from GaMD simulations was ~0.10, being consistent with the NMR experiments [129]. Additionally, the GaMD simulations suggested that POPC lipids in the lower leaflet of the inactive A_1AR system were less fluid than in the active A_1AR system. The similar -S_{CD} values of sn-2 acyl chains of POPC molecules in the upper leaflet were identified in the inactive and active A_1AR systems. However, the -S_{CD} for the lower leaflet in the inactive A_1AR system was larger than those in the active A_1AR system. This finding correlated well with the TM6 outward movement in the active A_1AR, which caused higher inclination of the C-H bonds to be aligned along the bilayer normal. In summary, GaMD simulations have revealed strongly coupled dynamics between a GPCR and the membrane lipids that depend on the receptor activation state.
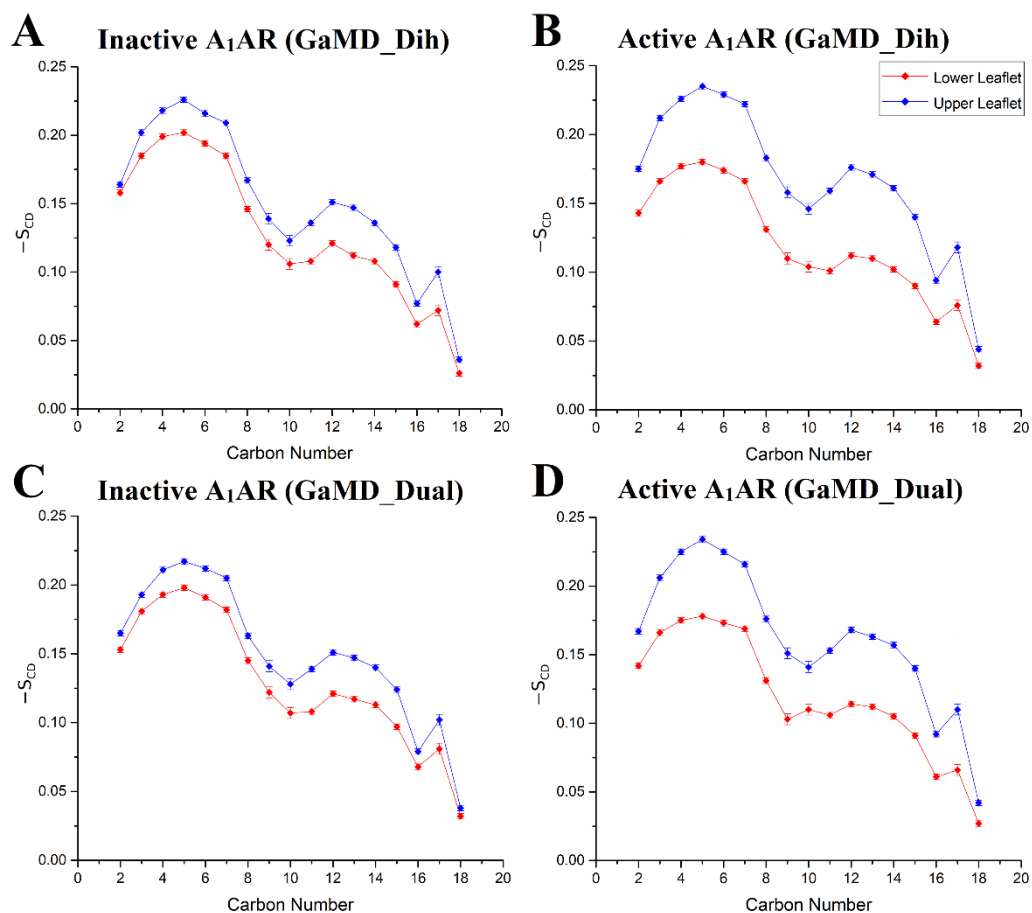

Figure 6. Differentiated order parameters of lipid molecules were found in simulation systems of the inactive and active A_1AR: (**A**) inactive A_1AR using dihedral-boost GaMD, (**B**) active A_1AR using dihedral-boost GaMD, (**C**) inactive A_1AR using dual-boost GaMD and (**D**) active A_1AR using dual-boost GaMD. Red diamond lines represent the average -S_{CD} order parameters for the cytoplasmic lower leaflet and blue diamond lines for the extracellular upper leaflet. Reprinted from reference [128] with permission from Wiley.

MD simulations were also performed to explore the effects of different lipids in antagonist caffeine binding to $A_{2A}AR$ [130]. Only POPC, a mixture of POPC and 1-palmitoyl-2-oleoyl-sn-glycero-3-phosphatidylethanolamine (POPE), and cholesterol rich lipid environment were used in the study. Simulations showed that H8 folding depended on the lipid environment. Cholesterol was observed to bind a cleft between TM1 and TM2, which stabilized a distinct caffeine binding pose. This further highlighted the importance of using physiological cholesterol concentration in MD simulations. Recently, Bruzzese et al. performed MD simulations to study the role of different lipids in activation of $A_{2A}AR$ [131]. Inactive $A_{2A}AR$ in the *apo* or agonist (ADO or NECA) bound conformations were used as starting structures in either 1,2-dioleoyl-sn-glycerol-3-phosphoglycerol (DOPG) or 1,2-dioleoyl-sn-glycerol-3-phosphocholine (DOPC) lipid bilayer. DOPC could facilitate the transition of the inactive $A_{2A}AR$ to an intermediate conformation. In DOPG with *apo* conformation of $A_{2A}AR$, the receptor could also transit to an intermediate conformation. Interestingly, the agonist-bound $A_{2A}AR$ transitioned into a fully active state. These variations were attributed to the allosteric effects mediated by the lipid and presence/absence of an agonist. Leonard et al. performed 35 µs MD simulations to study the preference for lipid solvation in the $A_{2A}AR$ [132]. Free energy of lipid solvation was calculated for different activation states of $A_{2A}AR$ with different lipids. The results showed that the inactive state preferred unsaturated lipids over the saturated ones for formation of the first solvation lipid shell around the receptor. This preference enhanced even more in the partially active $A_{2A}AR$ state as compared to that of the inactive receptor.

In addition to the above-mentioned all-atom MD simulations, coarse-grained models were also widely used to reach longer time scale and/or simulate larger systems. For example, both all-atom and coarse-grained MD simulations were performed to study the effects of membrane lipids and cations in the inactive, intermediate and fully active G protein-bound conformations of $A_{2A}AR$ [133]. The study was performed in both detergent micelles and lipid bilayer environment. MD simulations suggested that phosphatidylinositol bisphosphate 2 (PIP2) interacted with the $A_{2A}AR$ intracellular residues, which could reduce the flexibility of the receptor in the inactive state and limit the transition to the active-intermediate state. For the fully active $A_{2A}AR$, PIP2 stabilized the receptor–G protein complex. However, such stabilizing interactions were absent in the non-ionic micelles. The level of activation microswitches observed in the POPC lipid bilayer and detergent micelles were different, suggesting a rheostat model of GPCR activation microswitches as compared to a binary switch model. Song et al. [134] used coarse-grained MD simulations to study $A_{2A}AR$-lipid interactions. Simulations showed that different kinds of lipids could interact with nine binding sites on the receptor. The lipids were observed to allosterically modulate activation of $A_{2A}AR$. PIP2 could help stabilize the active state of the $A_{2A}AR$ by stabilizing outward movement of TM6 and enhancing the AR-G protein interactions. These studies strengthened the notion that lipids affect GPCR signaling and function by allosterically modulating its membrane lipid environment, being consistent with experimental findings [135]. For example, Huang et al. [135] identified cholesterol as a weak PAM of the $A_{2A}AR$ by combining [9]F NMR, computational analysis and G protein assays. Their GTP hydrolysis assays showed a marginal increase in basal activity with increasing cholesterol, in addition to a weak enhancement in the agonist potency. Furthermore, their ^{19}F NMR data suggested that the enhancement resulted from an increase in the receptor's active state population and a G protein-bound pre-coupled state.

3. Computer-Aided Drug Discovery of Adenosine Receptors

More than 515 million compounds are available in the ZINC chemical database [136]. It is impossible to perform high-throughput screening of all the chemical compounds. In this regard, virtual screening is a valuable strategy to efficiently screen a large number of compounds and select only a small subset of promising compounds for testing in in vitro and in vivo experiments [31,137,138]. Rodríguez et al. [139] identified 20 potent ligands by molecular docking from a pool of more than 6.7 million commercially available com-

pounds [139]. MD simulations have been incorporated into virtual screening to increase its success rate by providing a more reliable receptor structural ensemble and more accurate binding free energy calculation. In the following, we discuss novel binding site identification and drug design of ARs.

3.1. Drug Binding Sites of Adenosine Receptors

The orthosteric site has long been targeted to design drugs for ARs. However, this site is usually conserved across four subtypes of ARs. Consequently, it is critical to identify novel, less conserved binding sites to design selective ligands of ARs. Caliman et al. [140] used FTPMap to identify potential binding sites of the $A_{2A}AR$ in the 20 $A_{2A}AR$ crystal structures and 30 receptor clusters with 1.57 μs and 1.75 μs MD simulations of the *apo* receptor generated from structures of 3EML and 3QAK. Five "non-orthosteric" sites were identified, including the extracellular region of TM3 and TM4, lipid interface of TM5 and TM6, intracellular region between TM1 and TM7, G protein binding site among TM2, TM3, TM6 and TM7 and intracellular region of TM3 and TM4 [140].

Another method, the site-identification by ligand competitive saturation (SILCS) [141,142] method, was also developed to predict the location and approximate affinities of small molecular fragments on a target receptor surface by performing MD simulations. Moreover, MD simulations and mutation experiments were combined to identify residue hotspots of ARs for ligand binding. Wang et al. [143] explored the importance of specific residue hotspots by mutating Leu$^{6.51}$ to Val specific to the $A_{2B}AR$ in the $A_{2A}AR$. They incorporated MD simulations and radioligand binding assays to validate the mutation. A selective $A_{2A}AR$ antagonist ZM241385 indicated decreased affinity for the L249V$^{6.51}$ mutant of $A_{2A}AR$, suggesting the important role of this Leucine residue.

3.2. Binding Free Energy Calculations of Adenosine Receptors

One of the fundamental assumptions of ligand-based drug design is that similar molecules will have similar biological activity. Such an approach often fails when a small change in the ligand structure leads to a drastic difference in binding affinity [144]. In this regard, MD simulation and binding free energy calculation methods, including molecular mechanics Poisson–Boltzmann surface area (MM/PBSA), molecular mechanics generalized Born surface area (MM/GBSA) and free energy perturbation (FEP), have become valuable tools to predict ligand binding affinities for drug design [145,146]. MM/PBSA and MM/GBSA are popular methods for binding free energy prediction in drug design since they are more accurate than most scoring functions of molecular docking [146]. For example, Lenselink et al. [147] identified two ligands of $A_{2A}AR$ by applying MM/GBSA to rescore binding poses from Glide docking. Compared with MM/PBSA or MM/GBSA, MD/FEP is a more accurate binding free energy calculation method. Therefore, MD/FEP has been routinely used in drug design projects [45,145,148–152]. For the $A_{2A}AR$, MD/FEP calculations suggested the loss of binding of 3-deazaadenosine due to modification of a single heavy atom in ADO [150]. Even for such a small modification, MD/FEP was able to successfully predict the change of ligand binding affinity. One lead compound predicted from MD/FEP was synthesized and experimentally verified to be a full agonist equipotent to ADO. Furthermore, MD/FEP suggested that water in the binding site provided a major driving force for the ligand–protein interaction.

Fragment-based drug discovery relies on successful optimization of weak ligands for binding affinity and selectivity. MD/FEP has been widely applied in the fragment-to-lead optimization process. Matricon et al. [149] discovered that the benzothiazole fragment bound to the A_1AR through hydrogen bond interactions with N$^{6.55}$. Through a single vector growth, they designed nine additional compounds from the initial fragment, all of which showed improved binding affinity as suggested by MD/FEP calculations [149]. Eventually, the compounds were synthesized and their binding affinities in the A_1AR were experimentally measured by radioligand binding assays [149]. The resulting ligands led to >1000-fold improvements of binding affinity and nearly 40-fold higher subtype selectivity.

Furthermore, MD/FEP has been used to identify the ligand binding pose. In a proof-of-concept study, Jespers et al. [45] presented a robust protocol based on iterations of MD/FEP calculations, chemical synthesis, biophysical mapping and structural biology to determine the binding pose of a series of antagonists in the $A_{2A}AR$. Eight binding site mutations in the $A_{2A}AR$ were initially analyzed with MD/FEP calculations. The suggested ligand binding pose was subsequently used to guide the design of the new analogues. Remarkably, the binding affinities obtained from MD/FEP prediction were highly consistent with the experimental data. Furthermore, the predicted binding poses were highly consistent with the experimental structures.

3.3. Design of Biased Agonists of Adenosine Receptors

Wall et al. [106] discovered biased agonist BnOCPA of A_1AR that favors G_{ob} over other G protein subtypes and hence produces analgesic effects without sedation, bradycardia and hypotension. MD simulations revealed the BnOCPA binding modes in the receptor. BnOCPA binding resulted in unique active- and inactive-like conformations of the receptor during the simulations. Similarly, Baltos et al. [153] investigated the A_3AR biased agonists and discovered that several methyluronamide nucleoside derivatives exhibited biased agonism. In particular, molecular docking of MRS5679, an (*N*)-methanocarba nucleoside derivative with an extended C2 substituent, to a homology model of the A_3AR provided important insights into the molecular mechanism of biased signaling. Binding of the MRS5679 biased agonist favored a distinct conformation of the A_3AR with outward movement of the TM2 extracellular domain. Valant et al. [109] combined the endogenous agonist and allosteric modulator to design a bitopic ligand VCP746 as a biased agonist of A_1AR that favored cAMP pathway over ERK1/2 phosphorylation pathway. Molecular docking calculations and SuMD simulations [110,154] were used to study ligand binding to the receptor (see Section 3.4).

3.4. Design of Allosteric Modulators of Adenosine Receptors

Virtual screening has been widely used for agonist/antagonist design targeting GPCRs [31]. However, it is rather challenging to apply virtual screening to discover allosteric modulators with high potency. This is largely due to the lower affinity of allosteric modulators compared with the agonists/antagonists and high receptor flexibility of the target sites. Induced-fit docking [155] and ensemble docking [156] have been developed to account for receptor flexibility in virtual screening. The structural ensembles of target receptors could be taken from NMR structures, homology modeling, MD simulations or any other conformational sampling method [156–159]. It has been applied in AR allosteric modulator design. The receptor structural ensemble is often generated from MD simulations. Particularly, enhanced sampling MD simulations could sample larger conformational space of the drug target and have thus been shown to increase the success rate of finding allosteric modulators of the M_2 muscarinic GPCR [160]. In a recent study [161], we tested whether the receptor ensemble generated from GaMD simulations could increase the docking accuracy of discovering PAMs in the A_1AR. Extensive retrospective ensemble docking calculations of PAM binding to the A_1AR were performed using GaMD simulations and *AutoDock* (Figure 7) [162]. The dihedral and dual boost GaMD implemented in the AMBER and NAMD were performed. The rigid-body docking at short, medium and long levels and flexible docking were all evaluated in the ensemble docking protocol. The boost potential obtained for the same system with AMBER was larger than with NAMD in the GaMD simulations, which is due to different algorithms used to calculate the system potential statistics [112]. Accordingly, larger conformation space of the receptor was sampled in the AMBER simulations, leading to improved docking performance. Correction of docking score by the GaMD reweighted free energy of the receptor structural cluster further improved the docking performance. With GaMD reweighted scores, ranking by the average binding energy (BE_{avg}) performed better than by the minimum binding energy (BE_{min}) in terms of the area under the receiver operating characteristic curves (AUC), enrichment

factors (EFs) metrics. The receptor ensemble obtained from AMBER dual boost GaMD simulations of the VCP171 PAM-bound ADO-A_1AR-Gi outperformed other receptor ensembles for docking. This ensemble consisted of conformations of the *holo* A_1AR with PAM bound at the ECL2 allosteric site. Interactions between the PAM and receptor ECL2 might induce more reliable conformations for PAM binding, which were otherwise difficult to sample in the simulations of PAM-free (*apo*) A_1AR. Ensembles obtained from dual boost GaMD performed better than the dihedral-boost GaMD for docking, suggesting that GaMD with a higher acceleration level was needed to sufficiently sample conformational space of the GPCR PAM binding site.
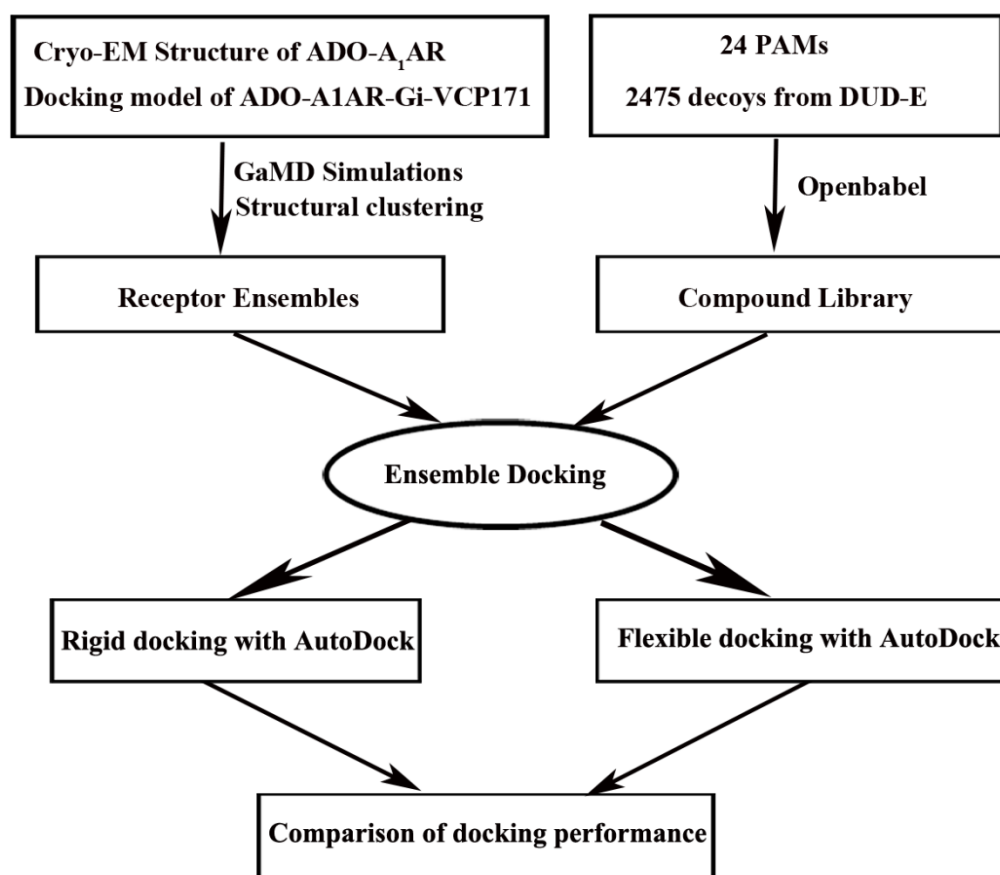
Figure 7. Overview flowchart for retrospective docking of positive allosteric modulators (PAMs) in the A_1AR: Starting from the cryo-EM structure of the active ADO-Gi-bound A_1AR (6D9H) and docking model of PAM VCP171-bound A_1AR (ADO-A_1AR-Gi-VCP171), GaMD simulations were carried out to construct structural ensembles to account for the receptor flexibility. Meanwhile, a compound library was prepared for 25 known PAMs of the A_1AR and 2475 decoys obtained from the DUD-E with *openbabel* 2.4.1. Ensemble docking was then performed to identify the PAMs for which the AUC and enrichment factors were calculated to evaluate docking performance. Both rigid-body and flexible docking were tested using *AutoDock*. Reprinted from reference [161] with permission from Elsevier.

Overall, flexible docking performed significantly better than the rigid-body docking at different levels with *AutoDock*. This suggested that the flexibility of protein side chains in ensemble docking also played an important role. The side chains of representative receptor structures obtained from GaMD simulations might be still in unfavored conformations for PAM binding. Flexible docking of protein side chains could then alleviate this problem to achieve better performance. In summary, GaMD simulations and flexible docking greatly improved the docking performance by effectively accounting for the protein flexibility

in both the backbone and side chains. Such an ensemble docking protocol will greatly facilitate future allosteric drug design of the A_1AR.

3.5. Design of Bitopic Ligands of Adenosine Receptors

Bitopic ligands contain hybrid molecular structures with pharmacophores of both orthosteric and allosteric ligands. Bitopic drug design has gained popularity because of its multivariate functions including increased efficacy and biased agonism in one ligand. Narlawar et al. [163] designed bitopic ligands of A_1AR combining orthosteric and allosteric pharmacophores with increasing length of linker between them. In particular, LUF6258 with a 9-carbon atom spacer between the allosteric and orthosteric moieties stood out with increased efficacy. The homology model of the A_1AR was used for docking of compounds and the binding poses were analyzed. LUF6258 had its adenosine part in the orthosteric pocket, whereas the allosteric moiety could extend out to the extracellular space and interacted with the ECL2 region. Valant et al. [109] rationally designed a new bitopic ligand VCP746 by combining endogenous agonist adenosine and PAM VCP171. VCP746, in an A_1AR-mediated inhibition assay, showed 30-fold biased agonism toward cAMP pathway in comparison to ERK1/2 phosphorylation pathway. In a follow up study [154], structural changes were made to VCP746, and structural–activity relationship experiments suggested that the 4-(trifluoromethyl) phenyl allosteric pharmacophore group was responsible for the ligand bias effect in A_1AR. Docking calculations using the A_1AR homology model suggested that the allosteric and linker region of the bitopic ligand explored the extracellular vestibule of the receptor. Deganutti et al. [110] applied SuMD to simulate the binding of VCP746 to A_1AR and proposed the binding modes of the bitopic ligand. The adenosine moiety of the ligand bound stably at the orthosteric site, whereas the VCP171 part bound near the ECL2 region. These molecular details further helped understanding the functional mechanism of the bitopic ligand. These studies provide evidence that combining orthosteric and allosteric pharmacophores improves pharmacological drug properties such as on-target efficacy, biased agonism, less on-target side effects, etc.

4. Conclusions

ARs have served as established drug targets. Computer-aided structure-based drug design approach has proven useful as while traditional agonists and antagonists often induce adverse side effects, new paradigms have emerged to search for novel biased agonists and allosteric modulators that can serve as selective drug molecules of the ARs. In this regard, because the target sites of these new ligands often involve regions on the receptor surface, it is crucial to account for receptor flexibility in order to design potent drug molecules. Additionally, kinetics of ligand binding has recently been recognized to be potentially more relevant for drug design. In particular, the dissociation rate constant that determines the drug residence time appears to better correlate with drug efficacy than the binding free energy [164,165]. However, ligand kinetic rates are even more difficult to compute than the binding free energies, largely due to slow processes of ligand binding and dissociation over long time scales [165]. Remarkable advances in MD approaches and computer hardware have paved the way to capture the ligand binding/unbinding processes of ARs in molecular details [166], which is expected to play a more important role in drug design in the future. In this context, advanced computational platforms (e.g., ANTON 3 [167] and Deep Docking [168]) and improved simulation techniques, including the coarse-grained MD, FEP, ligand and peptide GaMD [169,170], SuMD [110], Meta-dynamics [93], machine learning [171] and deep learning [168,172,173], will continue to drive rational computer-aided design of more potent and selective drug molecules of ARs.

Author Contributions: Conceptualization, J.W., A.B. and Y.M.; methodology, J.W., A.B., H.N.D., S.A. and Y.M.; data collection and analysis, J.W., A.B., H.N.D. and S.A.; writing—original draft preparation, J.W., A.B., H.N.D. and S.A.; writing—review and editing, J.W., A.B., H.N.D., S.A. and Y.M.; visualization, J.W., A.B., H.N.D. and S.A.; supervision, Y.M. All authors have read and agreed to the published version of the manuscript.

Institutional Review Board Statement: Not applicable.

Informed Consent Statement: Not applicable.

Data Availability Statement: Not applicable.

Conflicts of Interest: The authors declare no conflict of interest.

Abbreviations

ADO	Adenosine
ARs	Adenosine receptors
GPCR	G protein-coupled receptor
AC	Adenylyl cyclase
PI3K	Phosphoinositide 3 kinase
MAPK	Mitogen-activated protein kinase
PKA	Protein kinase A
PKC	Protein kinase C
PD	Parkinson's disease
NMR	Nuclear Magnetic Resonance
cryo-EM	Cryo-electron microscopy
MD	Molecular dynamics
TM6	Transmembrane helix 6
H8	Helix 8
ECL	Extracellular loop
NECA	$5'$-N-carboxamidoadenosine
cMD	Conventional MD
MSM	Markov state model
GaMD	Gaussian accelerated molecular dynamics
MS1	Metastable state
CS1	Canonical state
SuMD	Supervised MD
PAM	Positive allosteric modulator
NAM	Negative allosteric modulator
XAC	Xanthine amine congener
HMA	5-(N,N-hexamethylene) amiloride
CFF	Caffeine
POPC	1-palmitoyl-2-oleoyl-glycero-3-phosphocholine
POPE	1-palmitoyl-2-oleoyl-sn-glycero-3-phosphatidylethanolamine
DOPG	1,2-dioleoyl-sn-glycerol-3-phosphoglycerol
DOPC	1,2-dioleoyl-sn-glycerol-3-phosphocholine
PIP2	Phosphatidylinositol bisphosphate 2
SILCS	Site-identification by ligand competitive saturation
MM/PBSA	Molecular mechanics Poisson–Boltzmann surface area
MM/GBSA	Molecular mechanics generalized Born surface area
FEP	Free energy perturbation
BE_{avg}	Average binding energy
BE_{min}	Minimum binding energy

AUC	Area under the receiver operating characteristic curves
EFs	Enrichment factors

References

1. Jacobson, K.; Gao, Z.-G. Adenosine receptors as therapeutic targets. *Nat. Rev. Drug Discov.* **2006**, *5*, 247–264. [CrossRef] [PubMed]
2. Salmaso, V.; Jacobson, K.A. Purinergic Signaling: Impact of GPCR Structures on Rational Drug Design. *ChemMedChem* **2020**, *15*, 1958–1973. [CrossRef] [PubMed]
3. Fredholm, B.B.; IJzerman, A.P.; Jacobson, K.A.; Klotz, K.N.; Linden, J. International Union of Pharmacology. XXV. Nomenclature and classification of adenosine receptors. *Pharmacol. Rev.* **2001**, *53*, 527–552.
4. Finan, C.; Gaulton, A.; Kruger, F.A.; Lumbers, R.T.; Shah, T.; Engmann, J.; Galver, L.; Kelley, R.; Karlsson, A.; Santos, R.; et al. The druggable genome and support for target identification and validation in drug development. *Sci. Transl. Med.* **2017**, *9*, eaag1166. [CrossRef] [PubMed]
5. Fredholm, B.B.; IJzerman, A.P.; Jacobson, K.A.; Linden, J.; Müller, C.E. International Union of Basic and Clinical Pharmacology. LXXXI. Nomenclature and classification of adenosine receptors—An update. *Pharmacol. Rev.* **2011**, *63*, 1–34. [CrossRef] [PubMed]
6. Lasley, R.D. Adenosine receptors and membrane microdomains. *Biochim. Biophys. Acta (BBA) Biomembr.* **2011**, *1808*, 1284–1289. [CrossRef] [PubMed]
7. Cunha, R. Adenosine as a neuromodulator and as a homeostatic regulator in the nervous system: Different roles, different sources and different receptors. *Neurochem. Int.* **2001**, *38*, 107–125. [CrossRef]
8. Fredholm, B.B.; Abbracchio, M.P.; Burnstock, G.; Daly, J.W.; Harden, T.K.; Jacobson, K.A.; Leff, P.; Williams, M. Nomenclature and classification of purinoceptors. *Pharmacol. Rev.* **1994**, *46*, 143–156.
9. Haskó, G.; Linden, J.; Cronstein, B.; Pacher, P. Adenosine receptors: Therapeutic aspects for inflammatory and immune diseases. *Nat. Rev. Drug Discov.* **2008**, *7*, 759–770. [CrossRef]
10. Paganelli, F.; Gaudry, M.; Ruf, J.; Guieu, R. Recent advances in the role of the adenosinergic system in coronary artery disease. *Cardiovasc. Res.* **2020**, *117*, 1284–1294. [CrossRef]
11. Varani, K.; Vincenzi, F.; Merighi, S.; Gessi, S.; Borea, P.A. Biochemical and Pharmacological Role of A_1 Adenosine Receptors and Their Modulation as Novel Therapeutic Strategy. In *Protein Reviews: Volume 19*; Atassi, M.Z., Ed.; Springer: Singapore, 2017; pp. 193–232.
12. Chandrasekaran, B.; Samarneh, S.; Jaber, A.M.Y.; Kassab, G.; Agrawal, N. Therapeutic Potentials of A2B Adenosine Receptor Ligands: Current Status and Perspectives. *Curr. Pharm. Des.* **2019**, *25*, 2741–2771. [CrossRef]
13. DeOliveira, C.C.; Caria, C.R.E.P.; Gotardo, E.M.F.; Ribeiro, M.; Gambero, A. Role of A_1 and A_{2A} adenosine receptor agonists in adipose tissue inflammation induced by obesity in mice. *Eur. J. Pharmacol.* **2017**, *799*, 154–159. [CrossRef] [PubMed]
14. Vijayan, D.; Young, A.; Teng, M.W.L.; Smyth, M.J. Targeting immunosuppressive adenosine in cancer. *Nat. Rev. Cancer* **2017**, *17*, 709–724. [CrossRef] [PubMed]
15. Boison, D.; Yegutkin, G.G. Adenosine Metabolism: Emerging Concepts for Cancer Therapy. *Cancer Cell* **2019**, *36*, 582–596. [CrossRef]
16. Gessi, S.; Merighi, S.; Fazzi, D.; Stefanelli, A.; Varani, K.; Borea, P.A. Adenosine receptor targeting in health and disease. *Expert Opin. Investig. Drugs* **2011**, *20*, 1591–1609. [CrossRef] [PubMed]
17. De Lera Ruiz, M.; Lim, Y.-H.; Zheng, J. Adenosine A_{2A} Receptor as a Drug Discovery Target. *J. Med. Chem.* **2014**, *57*, 3623–3650. [CrossRef]
18. Nazario, L.R.; da Silva, R.S.; Bonan, C.D. Targeting Adenosine Signaling in Parkinson's Disease: From Pharmacological to Non-pharmacological Approaches. *Front. Neurosci.* **2017**, *11*, 658. [CrossRef] [PubMed]
19. Dungo, R.; Deeks, E.D. Istradefylline: First Global Approval. *Drugs* **2013**, *73*, 875–882. [CrossRef]
20. Haskó, G.; Csóka, B.; Németh, Z.H.; Vizi, E.S.; Pacher, P. A2B adenosine receptors in immunity and inflammation. *Trends Immunol.* **2009**, *30*, 263–270. [CrossRef]
21. Kotańska, M.; Szafarz, M.; Mika, K.; Dziubina, A.; Bednarski, M.; Müller, C.E.; Sapa, J.; Kieć-Kononowicz, K. PSB 603—A known selective adenosine A2B receptor antagonist—Has anti-inflammatory activity in mice. *Biomed. Pharmacother.* **2020**, *135*, 111164. [CrossRef]
22. Eltzschig, H.K.; Sitkovsky, M.V.; Robson, S.C. Purinergic Signaling during Inflammation. *N. Engl. J. Med.* **2012**, *367*, 2322–2333. [CrossRef] [PubMed]
23. Basu, S.; Barawkar, D.A.; Ramdas, V.; Patel, M.; Waman, Y.; Panmand, A.; Kumar, S.; Thorat, S.; Naykodi, M.; Goswami, A.; et al. Design and synthesis of novel xanthine derivatives as potent and selective A2B adenosine receptor antagonists for the treatment of chronic inflammatory airway diseases. *Eur. J. Med. Chem.* **2017**, *134*, 218–229. [CrossRef] [PubMed]
24. Shen, Y.; Tang, G.; Gao, P.; Zhang, B.; Xiao, H.; Si, L.-Y. Activation of adenosine A2B receptor attenuates high glucose-induced apoptosis in H9C2 cells via PI3K/Akt signaling. *In Vitro Cell. Dev. Biol. Anim.* **2018**, *54*, 384–391. [CrossRef] [PubMed]
25. Baraldi, P.G.; Preti, D.; Borea, P.A.; Varani, K. Medicinal Chemistry of A_3 Adenosine Receptor Modulators: Pharmacological Activities and Therapeutic Implications. *J. Med. Chem.* **2012**, *55*, 5676–5703. [CrossRef]
26. Jacobson, K.A.; Klutz, A.M.; Tosh, D.K.; Ivanov, A.A.; Preti, D.; Baraldi, P.G. Medicinal chemistry of the A_3 adenosine receptor: Agonists, antagonists, and receptor engineering. In *Adenosine Receptors in Health and Disease*; Springer: Cham, Switzerland, 2009; pp. 123–159.

27. Antonioli, L.; Lucarini, E.; Lambertucci, C.; Fornai, M.; Pellegrini, C.; Benvenuti, L.; Mannelli, L.D.C.; Spinaci, A.; Marucci, G.; Blandizzi, C.; et al. The Anti-Inflammatory and Pain-Relieving Effects of AR170, an Adenosine A$_3$ Receptor Agonist, in a Rat Model of Colitis. *Cells* **2020**, *9*, 1509. [CrossRef]

28. Park, C.-W.; Han, C.-T.; Sakaguchi, Y.; Lee, J.; Youn, H.-Y. Safety evaluation of FM101, an A$_3$ adenosine receptor modulator, in rat, for developing as therapeutics of glaucoma and hepatitis. *EXCLI J.* **2020**, *19*, 187–200.

29. Pal, Y.; Bandyopadhyay, N.; Pal, R.S.; Ahmed, S.; Bandopadhyay, S. Perspective and Potential of A$_{2A}$ and A$_3$ Adenosine Receptors as Therapeutic Targets for the Treatment of Rheumatoid Arthritis. *Curr. Pharm. Des.* **2019**, *25*, 2859–2874. [CrossRef]

30. Coppi, E.; Dettori, I.; Cherchi, F.; Bulli, I.; Venturini, M.; Pedata, F.; Pugliese, A.M. New Insight into the Role of Adenosine in Demyelination, Stroke and Neuropathic Pain. *Front. Pharmacol.* **2021**, *11*, 625662. [CrossRef]

31. Wang, J.; Bhattarai, A.; Ahmad, W.I.; Farnan, T.S.; John, K.P.; Miao, Y. Computer-aided GPCR drug discovery. In *GPCRs*; Jastrzebska, B., Park, P.S.H., Eds.; Academic Press: Cambridge, MA, USA, 2020; pp. 283–293.

32. Sussman, J.L.; Lin, D.; Jiang, J.; Manning, N.O.; Prilusky, J.; Ritter, O.; Abola, E.E. Protein Data Bank (PDB): Database of Three-Dimensional Structural Information of Biological Macromolecules. *Acta Crystallogr. Sect. D Biol. Crystallogr.* **1998**, *54*, 1078–1084. [CrossRef]

33. Karplus, M.; McCammon, J.A. Molecular dynamics simulations of biomolecules. *Nat. Struct. Mol. Biol.* **2002**, *9*, 646–652. [CrossRef]

34. Beauglehole, A.R.; Baker, S.P.; Scammells, P.J. Fluorosulfonyl-Substituted Xanthines as Selective Irreversible Antagonists for the A1-Adenosine Receptor. *J. Med. Chem.* **2000**, *43*, 4973–4980. [CrossRef] [PubMed]

35. Glukhova, A.; Thal, D.M.; Nguyen, A.T.; Vecchio, E.A.; Jörg, M.; Scammells, P.J.; May, L.T.; Sexton, P.M.; Christopoulos, A. Structure of the Adenosine A$_1$ Receptor Reveals the Basis for Subtype Selectivity. *Cell* **2017**, *168*, 867–877.e13. [CrossRef]

36. Cheng, R.K.; Segala, E.; Robertson, N.; Deflorian, F.; Doré, A.S.; Errey, J.C.; Fiez-Vandal, C.; Marshall, F.H.; Cooke, R.M. Structures of Human A$_1$ and A$_{2A}$ Adenosine Receptors with Xanthines Reveal Determinants of Selectivity. *Structure* **2017**, *25*, 1275–1285.e4. [CrossRef] [PubMed]

37. Peet, N.P.; Lentz, N.L.; Meng, E.C.; Dudley, M.W.; Ogden, A.M.L.; Demeter, D.A.; Weintraub, H., Jr.; Bey, P. A novel synthesis of xanthines: Support for a new binding mode for xanthines with respect to adenosine at adenosine receptors. *J. Med. Chem.* **1990**, *33*, 3127–3130. [CrossRef]

38. Draper-Joyce, C.J.; Khoshouei, M.; Thal, D.M.; Liang, Y.-L.; Nguyen, A.T.; Furness, S.G.; Venugopal, H.; Baltos, J.-A.; Plitzko, J.M.; Danev, R. Structure of the adenosine-bound human adenosine A$_1$ receptor–G i complex. *Nature* **2018**, *558*, 559–563. [CrossRef]

39. Draper-Joyce, C.J.; Bhola, R.; Wang, J.; Bhattarai, A.; Nguyen, A.T.N.; Cowie-Kent, I.; O'Sullivan, K.; Chia, L.Y.; Venugopal, H.; Valant, C.; et al. Positive allosteric mechanisms of adenosine A$_1$ receptor-mediated analgesia. *Nature* **2021**, *597*, 571–576. [CrossRef]

40. Minetti, P.; Tinti, M.O.; Carminati, P.; Castorina, M.; Di Cesare, M.A.; Di Serio, S.; Gallo, G.; Ghirardi, O.; Giorgi, F.; Giorgi, L.; et al. 2-n-Butyl-9-methyl-8-[1,2,3]triazol-2-yl-9H-purin-6-ylamine and Analogues as A$_{2A}$ Adenosine Receptor Antagonists. Design, Synthesis, and Pharmacological Characterization. *J. Med. Chem.* **2005**, *48*, 6887–6896. [CrossRef]

41. Martynowycz, M.W.; Shiriaeva, A.; Ge, X.; Hattne, J.; Nannenga, B.L.; Cherezov, V.; Gonen, T. MicroED structure of the human adenosine receptor determined from a single nanocrystal in LCP. *Proc. Natl. Acad. Sci. USA* **2021**, *118*, e2106041118. [CrossRef] [PubMed]

42. Amelia, T.; van Veldhoven, J.P.D.; Falsini, M.; Liu, R.; Heitman, L.H.; van Westen, G.J.P.; Segala, E.; Verdon, G.; Cheng, R.K.Y.; Cooke, R.M.; et al. Crystal Structure and Subsequent Ligand Design of a Nonriboside Partial Agonist Bound to the Adenosine A$_{2A}$ Receptor. *J. Med. Chem.* **2021**, *64*, 3827–3842. [CrossRef] [PubMed]

43. Ihara, K.; Hato, M.; Nakane, T.; Yamashita, K.; Kimura-Someya, T.; Hosaka, T.; Ishizuka-Katsura, Y.; Tanaka, R.; Tanaka, T.; Sugahara, M.; et al. Isoprenoid-chained lipid EROCOC17+4: A new matrix for membrane protein crystallization and a crystal delivery medium in serial femtosecond crystallography. *Sci. Rep.* **2020**, *10*, 19305. [CrossRef]

44. Lee, M.-Y.; Geiger, J.; Ishchenko, A.; Han, G.W.; Barty, A.; White, T.; Gati, C.; Batyuk, A.; Hunter, M.S.; Aquila, A.; et al. Harnessing the power of an X-ray laser for serial crystallography of membrane proteins crystallized in lipidic cubic phase. *IUCrJ* **2020**, *7*, 976–984. [CrossRef] [PubMed]

45. Jespers, W.; Verdon, G.; Azuaje, J.; Majellaro, M.; Keränen, H.; García-Mera, X.; Congreve, M.; Deflorian, F.; De Graaf, C.; Zhukov, A.; et al. X-ray Crystallography and Free Energy Calculations Reveal the Binding Mechanism of A$_{2A}$ Adenosine Receptor Antagonists. *Angew. Chem. Int. Ed.* **2020**, *59*, 16536–16543. [CrossRef]

46. Nass, K.; Cheng, R.; Vera, L.; Mozzanica, A.; Redford, S.; Ozerov, D.; Basu, S.; James, D.; Knopp, G.; Cirelli, C.; et al. Advances in long-wavelength native phasing at X-ray free-electron lasers. *IUCrJ* **2020**, *7*, 965–975. [CrossRef] [PubMed]

47. Ishchenko, A.; Stauch, B.; Han, G.W.; Batyuk, A.; Shiriaeva, A.; Li, C.; Zatsepin, N.; Weierstall, U.; Liu, W.; Nango, E.; et al. Toward G protein-coupled receptor structure-based drug design using X-ray lasers. *IUCrJ* **2019**, *6*, 1106–1119. [CrossRef]

48. Shimazu, Y.; Tono, K.; Tanaka, T.; Yamanaka, Y.; Nakane, T.; Mori, C.; Kimura, K.T.; Fujiwara, T.; Sugahara, M.; Tanaka, R.; et al. High-viscosity sample-injection device for serial femtosecond crystallography at atmospheric pressure. *J. Appl. Crystallogr.* **2019**, *52*, 1280–1288. [CrossRef] [PubMed]

49. Borodovsky, A.; Barbon, C.M.; Wang, Y.; Ye, M.; Prickett, L.; Chandra, D.; Shaw, J.; Deng, N.; Sachsenmeier, K.; Clarke, J.D.; et al. Small molecule AZD4635 inhibitor of A$_{2A}$R signaling rescues immune cell function including CD103+ dendritic cells enhancing anti-tumor immunity. *J. Immunother. Cancer* **2020**, *8*, e000417. [CrossRef] [PubMed]

50. Martin-Garcia, J.M.; Zhu, L.; Mendez, D.; Lee, M.-Y.; Chun, E.; Li, C.; Hu, H.; Subramanian, G.; Kissick, D.; Ogata, C.; et al. High-viscosity injector-based pink-beam serial crystallography of microcrystals at a synchrotron radiation source. *IUCrJ* **2019**, *6*, 412–425. [CrossRef]

51. Volpini, R.; Costanzi, S.; Lambertucci, C.; Portino, F.R.; Taffi, S.; Vittori, S.; Klotz, K.-N.; Cristalli, G. Adenosine receptor agonists: Synthesis and binding affinity of 2- (aryl)alkylthioadenosine derivatives. *Arkivoc* **2004**, *2004*, 301–311. [CrossRef]

52. Nafria, J.G.; Lee, Y.; Bai, X.; Carpenter, B.; Tate, C.G. Cryo-EM structure of the adenosine A_{2A} receptor coupled to an engineered heterotrimeric G protein. *eLife* **2018**, *7*, e35946. [CrossRef]

53. White, K.L.; Eddy, M.T.; Gao, Z.-G.; Han, G.W.; Lian, T.; Deary, A.; Patel, N.; Jacobson, K.A.; Katritch, V.; Stevens, R.C. Structural Connection between Activation Microswitch and Allosteric Sodium Site in GPCR Signaling. *Structure* **2018**, *26*, 259–269.e5. [CrossRef]

54. Rucktooa, P.; Cheng, R.K.Y.; Segala, E.; Geng, T.; Errey, J.C.; Brown, G.A.; Cooke, R.M.; Marshall, F.H.; Doré, A.S. Towards high throughput GPCR crystallography: In Meso soaking of Adenosine A_{2A} Receptor crystals. *Sci. Rep.* **2018**, *8*, 41. [CrossRef] [PubMed]

55. Basu, S.; Barawkar, D.A.; Thorat, S.; Shejul, Y.D.; Patel, M.; Naykodi, M.; Jain, V.; Salve, Y.; Prasad, V.; Chaudhary, S.; et al. Design, Synthesis of Novel, Potent, Selective, Orally Bioavailable Adenosine A_{2A} Receptor Antagonists and Their Biological Evaluation. *J. Med. Chem.* **2017**, *60*, 681–694. [CrossRef] [PubMed]

56. Congreve, M.; Andrews, S.P.; Doré, A.S.; Hollenstein, K.; Hurrell, E.; Langmead, C.J.; Mason, J.S.; Ng, I.W.; Tehan, B.; Zhukov, A.; et al. Discovery of 1,2,4-Triazine Derivatives as Adenosine A_{2A} Antagonists using Structure Based Drug Design. *J. Med. Chem.* **2012**, *55*, 1898–1903. [CrossRef] [PubMed]

57. Sams, A.G.; Mikkelsen, G.K.; Larsen, M.; Langgård, M.; Howells, M.E.; Schrøder, T.J.; Brennum, L.T.; Torup, L.; Jørgensen, E.B.; Bundgaard, C.; et al. Discovery of Phosphoric Acid Mono-{2-[(E/Z)-4-(3,3-dimethyl-butyrylamino)-3,5-difluoro-benzoylimino]-thiazol-3-ylmethyl} Ester (Lu AA47070): A Phos-phonooxymethylene Prodrug of a Potent and Selective hA_{2A} Receptor Antagonist. *J. Med. Chem.* **2011**, *54*, 751–764. [CrossRef] [PubMed]

58. Eddy, M.T.; Lee, M.-Y.; Gao, Z.-G.; White, K.L.; Didenko, T.; Horst, R.; Audet, M.; Stanczak, P.; McClary, K.M.; Han, G.W.; et al. Allosteric Coupling of Drug Binding and Intracellular Signaling in the A_{2A} Adenosine Receptor. *Cell* **2018**, *172*, 68–80.e12. [CrossRef]

59. Broecker, J.; Morizumi, T.; Ou, W.-L.; Klingel, V.; Kuo, A.; Kissick, D.J.; Ishchenko, A.; Lee, M.-Y.; Xu, S.; Makarov, O.; et al. High-throughput in situ X-ray screening of and data collection from protein crystals at room temperature and under cryogenic conditions. *Nat. Protoc.* **2018**, *13*, 260–292. [CrossRef]

60. Weinert, T.; Olieric, N.; Cheng, R.; Brünle, S.; James, D.; Ozerov, D.; Gashi, D.; Vera, L.; Marsh, M.; Jaeger, K.; et al. Serial millisecond crystallography for routine room-temperature structure determination at synchrotrons. *Nat. Commun.* **2017**, *8*, 542. [CrossRef]

61. Zhukov, A.; Andrews, S.P.; Errey, J.C.; Robertson, N.; Tehan, B.; Mason, J.S.; Marshall, F.H.; Weir, M.; Congreve, M. Biophysical Mapping of the Adenosine A_{2A} Receptor. *J. Med. Chem.* **2011**, *54*, 4312–4323. [CrossRef]

62. Melnikov, I.; Polovinkin, V.; Kovalev, K.; Gushchin, I.; Shevtsov, M.; Shevchenko, V.; Mishin, A.; Alekseev, A.; Rodriguez-Valera, F.; Borshchevskiy, V.; et al. Fast iodide-SAD phasing for high-throughput membrane protein structure determination. *Sci. Adv.* **2017**, *3*, e1602952. [CrossRef]

63. Martin-Garcia, J.M.; Conrad, C.E.; Nelson, G.; Stander, N.; Zatsepin, N.A.; Zook, J.; Zhu, L.; Geiger, J.; Chun, E.; Kissick, D.; et al. Serial millisecond crystallography of membrane and soluble protein microcrystals using synchrotron radiation. *IUCrJ* **2017**, *4*, 439–454. [CrossRef]

64. Sun, B.; Bachhawat, P.; Chu, M.L.-H.; Wood, M.; Ceska, T.; Sands, Z.A.; Mercier, J.; Lebon, F.; Kobilka, T.S.; Kobilka, B.K. Crystal structure of the adenosine A_{2A} receptor bound to an antagonist reveals a potential allosteric pocket. *Proc. Natl. Acad. Sci. USA* **2017**, *114*, 2066–2071. [CrossRef] [PubMed]

65. Batyuk, A.; Galli, L.; Ishchenko, A.; Han, G.W.; Gati, C.; Popov, P.A.; Lee, M.-Y.; Stauch, B.; White, T.A.; Barty, A.; et al. Native phasing of x-ray free-electron laser data for a G protein–coupled receptor. *Sci. Adv.* **2016**, *2*, e1600292. [CrossRef] [PubMed]

66. Keeling, S.E.; Albinson, F.; Ayres, B.E.; Butchers, P.R.; Chambers, C.; Cherry, P.C.; Ellis, F.; Ewan, G.B.; Gregson, M.; Knight, J.; et al. The discovery and synthesis of highly potent, A_{2A} receptor agonists. *Bioorg. Med. Chem. Lett.* **2000**, *10*, 403–406. [CrossRef]

67. Carpenter, B.; Nehme, R.; Warne, T.; Leslie, A.G.; Tate, C.G. Structure of the adenosine A_{2A} receptor bound to an engineered G protein. *Nature* **2016**, *536*, 104–107. [CrossRef]

68. Segala, E.; Guo, D.; Cheng, R.K.Y.; Bortolato, A.; Deflorian, F.; Doré, A.S.; Errey, J.C.; Heitman, L.H.; Ijzerman, A.P.; Marshall, F.H.; et al. Controlling the Dissociation of Ligands from the Adenosine A_{2A} Receptor through Modulation of Salt Bridge Strength. *J. Med. Chem.* **2016**, *59*, 6470–6479. [CrossRef]

69. Matsuda, A.; Shinozaki, M.; Yamaguchi, T.; Homma, H.; Nomoto, R.; Miyasaka, T.; Watanabe, Y.; Abiru, T. Nucleosides and nucleotides. 103. 2-Alkynyladenosines: A novel class of selective adenosine A2 receptor agonists with potent antihypertensive effects. *J. Med. Chem.* **1992**, *35*, 241–252. [CrossRef]

70. Lebon, G.; Edwards, P.C.; Leslie, A.G.W.; Tate, C.G. Molecular Determinants of CGS21680 Binding to the Human Adenosine A_{2A} Receptor. *Mol. Pharmacol.* **2015**, *87*, 907–915. [CrossRef]

71. Liu, W.; Chun, E.; Thompson, A.A.; Chubukov, P.; Xu, F.; Katritch, V.; Han, G.W.; Roth, C.B.; Heitman, L.H.; Ijzerman, A.P.; et al. Structural Basis for Allosteric Regulation of GPCRs by Sodium Ions. *Science* **2012**, *337*, 232–236. [CrossRef]

72. Hino, T.; Arakawa, T.; Iwanari, H.; Yurugi-Kobayashi, T.; Ikeda-Suno, C.; Nakada-Nakura, Y.; Kusano-Arai, O.; Weyand, S.; Shimamura, T.; Nomura, N.; et al. G-protein-coupled receptor inactivation by an allosteric inverse-agonist antibody. *Nature* **2012**, *482*, 237–240. [CrossRef]

73. Doré, A.S.; Robertson, N.; Errey, J.C.; Ng, I.; Hollenstein, K.; Tehan, B.; Hurrell, E.; Bennett, K.; Congreve, M.; Magnani, F.; et al. Structure of the Adenosine A$_{2A}$ Receptor in Complex with ZM241385 and the Xanthines XAC and Caffeine. *Structure* **2011**, *19*, 1283–1293. [CrossRef]

74. Lebon, G.; Warne, T.; Edwards, P.C.; Bennett, K.; Langmead, C.J.; Leslie, A.G.W.; Tate, C.G. Agonist-bound adenosine A$_{2A}$ receptor structures reveal common features of GPCR activation. *Nature* **2011**, *474*, 521–525. [CrossRef] [PubMed]

75. Xu, F.; Wu, H.; Katritch, V.; Han, G.W.; Jacobson, K.A.; Gao, Z.-G.; Cherezov, V.; Stevens, R.C. Structure of an Agonist-Bound Human A$_{2A}$ Adenosine Receptor. *Science* **2011**, *332*, 322–327. [CrossRef] [PubMed]

76. Jaakola, V.-P.; Griffith, M.T.; Hanson, M.A.; Cherezov, V.; Chien, E.Y.T.; Lane, J.R.; Ijzerman, A.P.; Stevens, R.C. The 2.6 Angstrom Crystal Structure of a Human A$_{2A}$ Adenosine Receptor Bound to an Antagonist. *Science* **2008**, *322*, 1211–1217. [CrossRef]

77. Park, P.S.-H.; Lodowski, D.T.; Palczewski, K. Activation of G Protein–Coupled Receptors: Beyond Two-State Models and Tertiary Conformational Changes. *Annu. Rev. Pharmacol. Toxicol.* **2008**, *48*, 107–141. [CrossRef]

78. Trzaskowski, B.; Latek, D.; Yuan, S.; Ghoshdastider, U.; Debinski, A.; Filipek, S. Action of Molecular Switches in GPCRs—Theoretical and Experimental Studies. *Curr. Med. Chem.* **2012**, *19*, 1090–1109. [CrossRef] [PubMed]

79. Ballesteros, J.A.; Weinstein, H. Integrated methods for the construction of three-dimensional models and computational probing of structure-function relations in G protein-coupled receptors. *Methods Neurosci.* **1995**, *25*, 366–428.

80. Eddy, M.T.; Gao, Z.-G.; Mannes, P.; Patel, N.; Jacobson, K.A.; Katritch, V.; Stevens, R.C.; Wüthrich, K. Extrinsic Tryptophans as NMR Probes of Allosteric Coupling in Membrane Proteins: Application to the A$_{2A}$ Adenosine Receptor. *J. Am. Chem. Soc.* **2018**, *140*, 8228–8235. [CrossRef]

81. Sušac, L.; Eddy, M.T.; Didenko, T.; Stevens, R.C.; Wüthrich, K. A$_{2A}$ adenosine receptor functional states characterized by 19F-NMR. *Proc. Natl. Acad. Sci. USA* **2018**, *115*, 12733–12738. [CrossRef]

82. Rodríguez, D.; Piñeiro, A.; Gutiérrez-De-Terán, H. Molecular Dynamics Simulations Reveal Insights into Key Structural Elements of Adenosine Receptors. *Biochemistry* **2011**, *50*, 4194–4208. [CrossRef]

83. Caliman, A.D.; Swift, S.E.; Wang, Y.; Miao, Y.; McCammon, J.A. Investigation of the conformational dynamics of the apo A$_{2A}$ adenosine receptor. *Protein Sci.* **2015**, *24*, 1004–1012. [CrossRef]

84. Yuan, S.; Filipek, S.; Palczewski, K.; Vogel, H. Activation of G-protein-coupled receptors correlates with the formation of a continuous internal water pathway. *Nat. Commun.* **2014**, *5*, 4733. [CrossRef] [PubMed]

85. Yuan, S.; Hu, Z.; Filipek, S.; Vogel, H. W246(6.48) opens a gate for a continuous intrinsic water pathway during activation of the adenosine A$_{2A}$ receptor. *Angew. Chem. Int. Ed.* **2015**, *54*, 556–559.

86. Hollingsworth, S.A.; Dror, R.O. Molecular Dynamics Simulation for All. *Neuron* **2018**, *99*, 1129–1143. [CrossRef]

87. Johnston, J.M.; Filizola, M. Showcasing modern molecular dynamics simulations of membrane proteins through G protein-coupled receptors. *Curr. Opin. Struct. Biol.* **2011**, *21*, 552–558. [CrossRef] [PubMed]

88. Shaw, D.E.; Maragakis, P.; Lindorff-Larsen, K.; Piana, S.; Dror, R.O.; Eastwood, M.P.; Bank, J.A.; Jumper, J.M.; Salmon, J.K.; Shan, Y.; et al. Atomic-Level Characterization of the Structural Dynamics of Proteins. *Science* **2010**, *330*, 341–346. [CrossRef] [PubMed]

89. Vilardaga, J.-P.; Bünemann, M.; Krasel, C.; Castro, M.; Lohse, M. Measurement of the millisecond activation switch of G protein–coupled receptors in living cells. *Nat. Biotechnol.* **2003**, *21*, 807–812. [CrossRef] [PubMed]

90. Wang, J.; Arantes, P.R.; Bhattarai, A.; Hsu, R.V.; Pawnikar, S.; Huang, Y.M.; Palermo, G.; Miao, Y. Gaussian accelerated molecular dynamics (GaMD): Principles and applications. *Wiley Interdiscip. Rev. Comput. Mol. Sci.* **2021**, *11*, e1521. [CrossRef]

91. Spiwok, V.; Sucur, Z.; Hosek, P. Enhanced sampling techniques in biomolecular simulations. *Biotechnol. Adv.* **2015**, *33*, 1130–1140. [CrossRef]

92. Lovera, S.; Cuzzolin, A.; Kelm, S.; De Fabritiis, G.; Sands, Z.A. Reconstruction of apo A$_{2A}$ receptor activation pathways reveal ligand-competent intermediates and state-dependent cholesterol hotspots. *Sci. Rep.* **2019**, *9*, 14199. [CrossRef]

93. Li, J.; Jonsson, A.L.; Beuming, T.; Shelley, J.C.; Voth, G.A. Ligand-Dependent Activation and Deactivation of the Human Adenosine A$_{2A}$ Receptor. *J. Am. Chem. Soc.* **2013**, *135*, 8749–8759. [CrossRef]

94. Gao, Z.-G.; Inoue, A.; Jacobson, K.A. On the G protein-coupling selectivity of the native A2B adenosine receptor. *Biochem. Pharmacol.* **2017**, *151*, 201–213. [CrossRef] [PubMed]

95. Cordeaux, Y.; Ijzerman, A.P.; Hill, S.J. Coupling of the human A1adenosine receptor to different heterotrimeric G proteins: Evidence for agonist-specific G protein activation. *J. Cereb. Blood Flow Metab.* **2004**, *143*, 705–714. [CrossRef] [PubMed]

96. Cordeaux, Y.; Briddon, S.; Megson, A.E.; McDonnell, J.; Dickenson, J.; Hill, S. Influence of Receptor Number on Functional Responses Elicited by Agonists Acting at the Human Adenosine A$_1$ Receptor: Evidence for Signaling Pathway-Dependent Changes in Agonist Potency and Relative Intrinsic Activity. *Mol. Pharmacol.* **2000**, *58*, 1075–1084. [CrossRef] [PubMed]

97. Stewart, G.D.; Valant, C.; Dowell, S.J.; Mijaljica, D.; Devenish, R.J.; Scammells, P.J.; Sexton, P.M.; Christopoulos, A. Determination of Adenosine A$_1$ Receptor Agonist and Antagonist Pharmacology Using *Saccharomyces cerevisiae*: Implications for Ligand Screening and Functional Selectivity. *J. Pharmacol. Exp. Ther.* **2009**, *331*, 277–286. [CrossRef] [PubMed]

98. Lee, S.; Nivedha, A.K.; Tate, C.G.; Vaidehi, N. Dynamic Role of the G Protein in Stabilizing the Active State of the Adenosine A$_{2A}$ Receptor. *Structure* **2019**, *27*, 703–712.e3. [CrossRef] [PubMed]

99. Wang, J.; Miao, Y. Mechanistic Insights into Specific G Protein Interactions with Adenosine Receptors. *J. Phys. Chem. B* **2019**, *123*, 6462–6473. [CrossRef] [PubMed]
100. Baltos, J.-A.; Gregory, K.J.; White, P.J.; Sexton, P.; Christopoulos, A.; May, L.T. Quantification of adenosine A$_1$ receptor biased agonism: Implications for drug discovery. *Biochem. Pharmacol.* **2015**, *99*, 101–112. [CrossRef] [PubMed]
101. Vecchio, E.A.; Baltos, J.; Nguyen, A.T.N.; Christopoulos, A.; White, P.J.; May, L.T. New paradigms in adenosine receptor pharmacology: Allostery, oligomerization and biased agonism. *J. Cereb. Blood Flow Metab.* **2018**, *175*, 4036–4046. [CrossRef]
102. McNeill, S.M.; Baltos, J.-A.; White, P.J.; May, L.T. Biased agonism at adenosine receptors. *Cell. Signal.* **2021**, *82*, 109954. [CrossRef]
103. Jarpe, M.B.; Knall, C.; Mitchell, F.M.; Buhl, A.M.; Duzic, E.; Johnson, G.L. [d-Arg1,d-Phe5,d-Trp7,9,Leu11]Substance P Acts as a Biased Agonist toward Neuropeptide and Chemokine Receptors. *J. Biol. Chem.* **1998**, *273*, 3097–3104. [CrossRef]
104. Nagi, K.; Onaran, H.O. Biased agonism at G protein-coupled receptors. *Cell. Signal.* **2021**, *83*, 109981. [CrossRef]
105. Langemeijer, E.V.; Verzijl, D.; Dekker, S.J.; IJzerman, A.P. Functional selectivity of adenosine A$_1$ receptor ligands? *Purinergic Signal.* **2013**, *9*, 91–100. [CrossRef] [PubMed]
106. Wall, M.J.; Hill, E.; Huckstepp, R.; Barkan, K.; Deganutti, G.; Leuenberger, M.; Preti, B.; Winfield, I.; Wei, H.; Imlach, W.; et al. A biased adenosine A$_1$R agonist elicits analgesia without cardiorespiratory depression. *bioRxiv* **2020**. Available online: https://www.biorxiv.org/content/10.1101/2020.04.04.023945v3.full (accessed on 31 January 2022). [CrossRef]
107. Kato, H.E.; Zhang, Y.; Hu, H.; Suomivuori, C.-M.; Kadji, F.M.N.; Aoki, J.; Kumar, K.K.; Fonseca, R.; Hilger, D.; Huang, W. Conformational transitions of a neurotensin receptor 1–Gi1 complex. *Nature* **2019**, *572*, 80–85. [CrossRef]
108. Liu, X.; Xu, X.; Hilger, D.; Aschauer, P.; Tiemann, J.; Du, Y.; Liu, H.; Hirata, K.; Sun, X.; Guixà-González, R.; et al. Structural Insights into the Process of GPCR-G Protein Complex Formation. *Cell* **2019**, *177*, 1243–1251.e12. [CrossRef] [PubMed]
109. Valant, C.; May, L.T.; Aurelio, L.; Chuo, C.H.; White, P.J.; Baltos, J.-A.; Sexton, P.M.; Scammells, P.J.; Christopoulos, A. Separation of on-target efficacy from adverse effects through rational design of a bitopic adenosine receptor agonist. *Proc. Natl. Acad. Sci. USA* **2014**, *111*, 4614–4619. [CrossRef] [PubMed]
110. Deganutti, G.; Barkan, K.; Ladds, G.; Reynolds, C.A. Multisite Model of Allosterism for the Adenosine A$_1$ Receptor. *J. Chem. Inf. Model.* **2021**, *61*, 2001–2015. [CrossRef]
111. Gao, Z.-G.; Toti, K.S.; Campbell, R.; Suresh, R.R.; Yang, H.; Jacobson, K.A. Allosteric Antagonism of the A$_{2A}$ Adenosine Receptor by a Series of Bitopic Ligands. *Cells* **2020**, *9*, 1200. [CrossRef]
112. Miao, Y.; Bhattarai, A.; Nguyen, A.T.N.; Christopoulos, A.; May, L.T. Structural Basis for Binding of Allosteric Drug Leads in the Adenosine A$_1$ Receptor. *Sci. Rep.* **2018**, *8*, 16836. [CrossRef]
113. Case, D.A.; Aktulga, H.M.; Belfon, K.; Ben-Shalom, I.; Brozell, S.R.; Cerutti, D.; Cheatham, T., III; Cisneros, G.; Cruzeiro, V.; Darden, T. *Amber 2021*; University of California Press: Berkeley, CA, USA, 2021.
114. Phillips, J.C.; Braun, R.; Wang, W.; Gumbart, J.; Tajkhorshid, E.; Villa, E.; Chipot, C.; Skeel, R.D.; Kalé, L.; Schulten, K. Scalable molecular dynamics with NAMD. *J. Comput. Chem.* **2005**, *26*, 1781–1802. [CrossRef]
115. Nguyen, A.T.N.; Vecchio, E.A.; Thomas, T.; Nguyen, T.D.; Aurelio, L.; Scammells, P.J.; White, P.J.; Sexton, P.M.; Gregory, K.J.; May, L.T.; et al. Role of the Second Extracellular Loop of the Adenosine A$_1$ Receptor on Allosteric Modulator Binding, Signaling, and Cooperativity. *Mol. Pharmacol.* **2016**, *90*, 715–725. [CrossRef] [PubMed]
116. Deganutti, G.; Cuzzolin, A.; Ciancetta, A.; Moro, S. Understanding allosteric interactions in G protein-coupled receptors using Supervised Molecular Dynamics: A prototype study analysing the human A$_3$ adenosine receptor positive allosteric modulator LUF6000. *Bioorg. Med. Chem.* **2015**, *23*, 4065–4071. [CrossRef] [PubMed]
117. Bissaro, M.; Bolcato, G.; Deganutti, G.; Sturlese, M.; Moro, S. Revisiting the Allosteric Regulation of Sodium Cation on the Binding of Adenosine at the Human A$_{2A}$ Adenosine Receptor: Insights from Supervised Molecular Dynamics (SuMD) Simulations. *Molecules* **2019**, *24*, 2752. [CrossRef] [PubMed]
118. Guo, D.; Pan, A.C.; Dror, R.O.; Mocking, T.; Liu, R.; Heitman, L.H.; Shaw, D.E.; Ijzerman, A.P. Molecular Basis of Ligand Dissociation from the Adenosine A$_{2A}$ Receptor. *Mol. Pharmacol.* **2016**, *89*, 485–491. [CrossRef]
119. Deganutti, G.; Welihinda, A.; Moro, S. Comparison of the Human A$_{2A}$ Adenosine Receptor Recognition by Adenosine and Inosine: New Insight from Supervised Molecular Dynamics Simulations. *ChemMedChem* **2017**, *12*, 1319–1326. [CrossRef]
120. Sabbadin, D.; Ciancetta, A.; Deganutti, G.; Cuzzolin, A.; Moro, S. Exploring the recognition pathway at the human A$_{2A}$ adenosine receptor of the endogenous agonist adenosine using supervised molecular dynamics simulations. *MedChemComm* **2015**, *6*, 1081–1085. [CrossRef]
121. Bolcato, G.; Bissaro, M.; Deganutti, G.; Sturlese, M.; Moro, S. New Insights into Key Determinants for Adenosine 1 Receptor Antagonists Selectivity Using Supervised Molecular Dynamics Simulations. *Biomolecules* **2020**, *10*, 732. [CrossRef]
122. Deganutti, G.; Barkan, K.; Preti, B.; Leuenberger, M.; Wall, M.; Frenguelli, B.G.; Lochner, M.; Ladds, G.; Reynolds, C.A. Deciphering the Agonist Binding Mechanism to the Adenosine A$_1$ Receptor. *ACS Pharmacol. Transl. Sci.* **2021**, *4*, 314–326. [CrossRef]
123. Do, H.N.; Akhter, S.; Miao, Y. Pathways and Mechanism of Caffeine Binding to Human Adenosine A$_{2A}$ Receptor. *Front. Mol. Biosci.* **2021**, *8*, 673170. [CrossRef]
124. Khelashvili, G.; Grossfield, A.; Feller, S.E.; Pitman, M.C.; Weinstein, H. Structural and dynamic effects of cholesterol at preferred sites of interaction with rhodopsin identified from microsecond length molecular dynamics simulations. *Proteins* **2009**, *76*, 403–417. [CrossRef]
125. Khelashvili, G.; Albornoz, P.B.C.; Johner, N.; Mondal, S.; Caffrey, M.; Weinstein, H. Why GPCRs behave differently in cubic and lamellar lipidic mesophases. *J. Am. Chem. Soc.* **2012**, *134*, 15858–15868. [CrossRef]

126. Mondal, S.; Johnston, J.M.; Wang, H.; Khelashvili, G.; Filizola, M.; Weinstein, H. Membrane Driven Spatial Organization of GPCRs. *Sci. Rep.* **2013**, *3*, srep02909. [CrossRef] [PubMed]

127. Chachisvilis, M.; Zhang, Y.-L.; Frangos, J.A. G protein-coupled receptors sense fluid shear stress in endothelial cells. *Proc. Natl. Acad. Sci. USA* **2006**, *103*, 15463–15468. [CrossRef] [PubMed]

128. Bhattarai, A.; Wang, J.; Miao, Y. G-Protein-Coupled Receptor-Membrane Interactions Depend on the Receptor Activation State. *J. Comput. Chem.* **2020**, *41*, 460–471. [CrossRef] [PubMed]

129. Perly, B.; Smith, I.C.P.; Jarrell, H.C. Acyl chain dynamics of phosphatidylethanolamines containing oleic acid and dihydrosterculic acid: Deuteron NMR relaxation studies. *Biochemistry* **1985**, *24*, 4659–4665. [CrossRef] [PubMed]

130. Cao, R.; Rossetti, G.; Bauer, A.; Carioni, P. Binding of the Antagonist Caffeine to the Human Adenosine Receptor $hA_{2A}R$ in Nearly Physiological Conditions. *PLoS ONE* **2015**, *10*, e0126833. [CrossRef] [PubMed]

131. Bruzzese, A.; Dalton, J.A.R.; Giraldo, J. Insights into adenosine A_{2A} receptor activation through cooperative modulation of agonist and allosteric lipid interactions. *PLoS Comput. Biol.* **2020**, *16*, e1007818. [CrossRef]

132. Leonard, A.N.; Lyman, E. Activation of G-protein-coupled receptors is thermodynamically linked to lipid solvation. *Biophys. J.* **2021**, *120*, 1777–1787. [CrossRef]

133. Ma, N.; Lee, S.; Vaidehi, N. Activation Microswitches in Adenosine Receptor A_{2A} Function as Rheostats in the Cell Membrane. *Biochemistry* **2020**, *59*, 4059–4071. [CrossRef]

134. Song, W.; Yen, H.-Y.; Robinson, C.V.; Sansom, M.S. State-dependent Lipid Interactions with the A_{2A} Receptor Revealed by MD Simulations Using In Vivo-Mimetic Membranes. *Structure* **2018**, *27*, 392–403.e3. [CrossRef]

135. Huang, S.K.; Almurad, O.; Pejana, R.J.; Morrison, Z.A.; Pandey, A.; Picard, L.-P.; Nitz, M.; Sljoka, A.; Prosser, R.S. Allosteric modulation of the adenosine A_{2A} receptor by cholesterol. *eLife* **2022**, *11*, e73901. [CrossRef] [PubMed]

136. Irwin, J.J.; Tang, K.G.; Young, J.; Dandarchuluun, C.; Wong, B.R.; Khurelbaatar, M.; Moroz, Y.S.; Mayfield, J.; Sayle, R.A. ZINC20—A Free Ultralarge-Scale Chemical Database for Ligand Discovery. *J. Chem. Inf. Model.* **2020**, *60*, 6065–6073. [CrossRef] [PubMed]

137. Lavecchia, A.; Di Giovanni, C. Virtual screening strategies in drug discovery: A critical review. *Curr. Med. Chem.* **2013**, *20*, 2839–2860. [CrossRef] [PubMed]

138. Wang, G.; Zhu, W. Molecular docking for drug discovery and development: A widely used approach but far from perfect. *Future Med. Chem.* **2016**, *8*, 1707–1710. [CrossRef] [PubMed]

139. Rodríguez, D.; Gao, Z.-G.; Moss, S.M.; Jacobson, K.A.; Carlsson, J. Molecular Docking Screening Using Agonist-Bound GPCR Structures: Probing the A_{2A} Adenosine Receptor. *J. Chem. Inf. Model.* **2015**, *55*, 550–563. [CrossRef]

140. Caliman, A.D.; Miao, Y.; McCammon, J.A. Mapping the allosteric sites of the A_{2A} adenosine receptor. *Chem. Biol. Drug Des.* **2017**, *91*, 5–16. [CrossRef]

141. Yu, W.; Lakkaraju, S.K.; Raman, E.P.; Fang, L.; MacKerell, A.D., Jr. Pharmacophore modeling using site-identification by ligand competitive saturation (SILCS) with multiple probe molecules. *J. Chem. Inf. Model.* **2015**, *55*, 407–420. [CrossRef]

142. Raman, E.P.; Yu, W.; Lakkaraju, S.K.; MacKerell, A. Inclusion of Multiple Fragment Types in the Site Identification by Ligand Competitive Saturation (SILCS) Approach. *J. Chem. Inf. Model.* **2013**, *53*, 3384–3398. [CrossRef]

143. Wang, X.; Jespers, W.; Prieto-Díaz, R.; Majellaro, M.; Ijzerman, A.P.; van Westen, G.J.P.; Sotelo, E.; Heitman, L.H.; Gutiérrez-De-Terán, H. Identification of V6.51L as a selectivity hotspot in stereoselective A2B adenosine receptor antagonist recognition. *Sci. Rep.* **2021**, *11*, 14171. [CrossRef]

144. Ferenczy, G.G.; Keserű, G.M. Thermodynamics guided lead discovery and optimization. *Drug Discov. Today* **2010**, *15*, 919–932. [CrossRef]

145. Cournia, Z.; Allen, B.; Sherman, W. Relative Binding Free Energy Calculations in Drug Discovery: Recent Advances and Practical Considerations. *J. Chem. Inf. Model.* **2017**, *57*, 2911–2937. [CrossRef] [PubMed]

146. Wang, E.; Sun, H.; Wang, J.; Wang, Z.; Liu, H.; Zhang, J.Z.H.; Hou, T. End-Point Binding Free Energy Calculation with MM/PBSA and MM/GBSA: Strategies and Applications in Drug Design. *Chem. Rev.* **2019**, *119*, 9478–9508. [CrossRef] [PubMed]

147. Lenselink, E.B.; Beuming, T.; Van Veen, C.; Massink, A.; Sherman, W.; Van Vlijmen, H.W.T.; Ijzerman, A.P. In search of novel ligands using a structure-based approach: A case study on the adenosine A_{2A} receptor. *J. Comput. Mol. Des.* **2016**, *30*, 863–874. [CrossRef] [PubMed]

148. Keränen, H.; de Terán, H.G.; Åqvist, J. Structural and Energetic Effects of A_{2A} Adenosine Receptor Mutations on Agonist and Antagonist Binding. *PLoS ONE* **2014**, *9*, e108492. [CrossRef]

149. Matricon, P.; Vo, D.D.; Gao, Z.-G.; Kihlberg, J.; Jacobson, K.A.; Carlsson, J. Fragment-based design of selective GPCR ligands guided by free energy simulations. *Chem. Commun.* **2021**, *57*, 12305–12308. [CrossRef] [PubMed]

150. Matricon, P.; Suresh, R.R.; Gao, Z.-G.; Panel, N.; Jacobson, K.A.; Carlsson, J. Ligand design by targeting a binding site water. *Chem. Sci.* **2020**, *12*, 960–968. [CrossRef]

151. Deflorian, F.; Perez-Benito, L.; Lenselink, E.B.; Congreve, M.; Van Vlijmen, H.W.T.; Mason, J.S.; De Graaf, C.; Tresadern, G. Accurate Prediction of GPCR Ligand Binding Affinity with Free Energy Perturbation. *J. Chem. Inf. Model.* **2020**, *60*, 5563–5579. [CrossRef]

152. Cappel, D.; Hall, M.L.; Lenselink, E.B.; Beuming, T.; Qi, J.; Bradner, J.; Sherman, W. Relative Binding Free Energy Calculations Applied to Protein Homology Models. *J. Chem. Inf. Model.* **2016**, *56*, 2388–2400. [CrossRef]

153. Baltos, J.-A.; Paoletta, S.; Nguyen, A.T.N.; Gregory, K.J.; Tosh, D.K.; Christopoulos, A.; Jacobson, K.A.; May, L.T. Structure-Activity Analysis of Biased Agonism at the Human Adenosine A$_3$ Receptor. *Mol. Pharmacol.* **2016**, *90*, 12–22. [CrossRef]

154. Aurelio, L.; Baltos, J.-A.; Ford, L.; Nguyen, A.T.N.; Jörg, M.; Devine, S.M.; Valant, C.; White, P.J.; Christopoulos, A.; May, L.T.; et al. A Structure–Activity Relationship Study of Bitopic N6-Substituted Adenosine Derivatives as Biased Adenosine A$_1$ Receptor Agonists. *J. Med. Chem.* **2018**, *61*, 2087–2103. [CrossRef]

155. Sherman, W.; Day, T.; Jacobson, M.P.; Friesner, R.A.; Farid, R. Novel Procedure for Modeling Ligand/Receptor Induced Fit Effects. *J. Med. Chem.* **2005**, *49*, 534–553. [CrossRef] [PubMed]

156. Amaro, R.E.; Baudry, J.; Chodera, J.; Demir, Ö.; McCammon, J.A.; Miao, Y.; Smith, J.C. Ensemble Docking in Drug Discovery. *Biophys. J.* **2018**, *114*, 2271–2278. [CrossRef] [PubMed]

157. Bonvin, A.M. Flexible protein–protein docking. *Curr. Opin. Struct. Biol.* **2006**, *16*, 194–200. [CrossRef] [PubMed]

158. Dominguez, C.; Bonvin, A.M.; Winkler, G.S.; van Schaik, F.M.; Timmers, H.T.M.; Boelens, R. Structural Model of the UbcH5B/CNOT4 Complex Revealed by Combining NMR, Mutagenesis, and Docking Approaches. *Structure* **2004**, *12*, 633–644. [CrossRef]

159. Novoa, E.M.; De Pouplana, L.R.; Barril, X.; Orozco, M.; López, M.O. Ensemble Docking from Homology Models. *J. Chem. Theory Comput.* **2010**, *6*, 2547–2557. [CrossRef]

160. Miao, Y.; Goldfeld, D.A.; Von Moo, E.; Sexton, P.M.; Christopoulos, A.; McCammon, J.A.; Valant, C. Accelerated structure-based design of chemically diverse allosteric modulators of a muscarinic G protein-coupled receptor. *Proc. Natl. Acad. Sci. USA* **2016**, *113*, E5675–E5684. [CrossRef]

161. Bhattarai, A.; Wang, J.; Miao, Y. Retrospective ensemble docking of allosteric modulators in an adenosine G-protein-coupled receptor. *Biochim. Biophys. Acta (BBA) Gen. Subj.* **2020**, *1864*, 129615. [CrossRef]

162. Morris, G.M.; Huey, R.; Lindstrom, W.; Sanner, M.F.; Belew, R.K.; Goodsell, D.S.; Olson, A.J. AutoDock4 and AutoDockTools4: Automated docking with selective receptor flexibility. *J. Comput. Chem.* **2009**, *30*, 2785–2791. [CrossRef]

163. Narlawar, R.; Lane, J.R.; Doddareddy, M.; Lin, J.; Brussee, J.; Ijzerman, A.P. Hybrid Ortho/Allosteric Ligands for the Adenosine A$_1$ Receptor. *J. Med. Chem.* **2010**, *53*, 3028–3037. [CrossRef]

164. Schuetz, D.A.; de Witte, W.; Wong, Y.C.; Knasmueller, B.; Richter, L.; Kokh, D.B.; Sadiq, S.K.; Bosma, R.; Nederpelt, I.; Heitman, L.H.; et al. Kinetics for Drug Discovery: An industry-driven effort to target drug residence time. *Drug Discov. Today* **2017**, *22*, 896–911. [CrossRef]

165. Tonge, P.J. Drug–Target Kinetics in Drug Discovery. *ACS Chem. Neurosci.* **2017**, *9*, 29–39. [CrossRef]

166. Pawnikar, S.; Bhattarai, A.; Wang, J.; Miao, Y. Binding Analysis Using Accelerated Molecular Dynamics Simulations and Future Perspectives. *Adv. Appl. Bioinform. Chem.* **2022**, *15*, 1–19. [CrossRef] [PubMed]

167. Shaw, D.E.; Adams, P.J.; Azaria, A.; Bank, J.A.; Batson, B.; Bell, A.; Bergdorf, M.; Bhatt, J.; Butts, J.A.; Correia, T. Anton 3: Twenty microseconds of molecular dynamics simulation before lunch. In Proceedings of the International Conference for High Performance Computing, Networking, Storage and Analysis, St. Louis, MO, USA, 14–19 November 2021; pp. 1–11.

168. Gentile, F.; Agrawal, V.; Hsing, M.; Ton, A.-T.; Ban, F.; Norinder, U.; Gleave, M.E.; Cherkasov, A. Deep Docking: A Deep Learning Platform for Augmentation of Structure Based Drug Discovery. *ACS Cent. Sci.* **2020**, *6*, 939–949. [CrossRef] [PubMed]

169. Wang, J.; Miao, Y. Peptide Gaussian accelerated molecular dynamics (Pep-GaMD): Enhanced sampling and free energy and kinetics calculations of peptide binding. *J. Chem. Phys.* **2020**, *153*, 154109. [CrossRef] [PubMed]

170. Miao, Y.; Bhattarai, A.; Wang, J. Ligand Gaussian Accelerated Molecular Dynamics (LiGaMD): Characterization of Ligand Binding Thermodynamics and Kinetics. *J. Chem. Theory Comput.* **2020**, *16*, 5526–5547. [CrossRef]

171. Zhao, L.; Ciallella, H.L.; Aleksunes, L.M.; Zhu, H. Advancing computer-aided drug discovery (CADD) by big data and data-driven machine learning modeling. *Drug Discov. Today* **2020**, *25*, 1624–1638. [CrossRef]

172. Wang, M.; Hou, S.; Wei, Y.; Li, D.; Lin, J. Discovery of novel dual adenosine A$_1$/A$_{2A}$ receptor antagonists using deep learning, pharmacophore modeling and molecular docking. *PLoS Comput. Biol.* **2021**, *17*, e1008821. [CrossRef]

173. Liu, X.; Ye, K.; Van Vlijmen, H.W.T.; Ijzerman, A.P.; Van Westen, G.J.P. An exploration strategy improves the diversity of de novo ligands using deep reinforcement learning: A case for the adenosine A$_{2A}$ receptor. *J. Cheminf.* **2019**, *11*, 35. [CrossRef]